Nonlinear Dyn
https://doi.org/10.1007/s11071-025-10917-7

RESEARCH

Stochastic modeling of COVID-19 spread in India: an approach incorporating logarithmic mean-reverting Ornstein-Uhlenbeck process with two-dose vaccine impact analysis

T. A. Midhun · Sayooj Aby Jose · K. Murugesan · Anuwat Jirawattanapanit

Received: 21 November 2024 / Accepted: 19 January 2025

Abstract The COVID-19 pandemic has introduced unparalleled challenges worldwide, highlighting the need for sophisticated models to understand its dynamics. In this study, we present a comprehensive analysis of a stochastic model incorporating dual doses of vaccine and the logarithmic mean-reverting Ornstein-Uhlenbeck process to analyze the dynamics of SARS-CoV-2 (the virus responsible for COVID-19) infection in India. The study begins with constructing a deterministic model and then it is extended to a stochastic framework. Firstly, we perform a thorough analysis of the deterministic model to confirm the existence and uniqueness of a globally positive solution, ensuring that it remains bounded. Additionally, the basic reproduction number R_0^d is derived and the local asymptotic stability of the disease-free equilibrium is evaluated under the condition $R_0^d < 1$. Next, we analyze the formulated stochastic model and identify two critical threshold parameters, R_0^e and R_0^s. Specifically, $R_0^e < 1$ indicates exponential extinction of the infection, whereas $R_0^s > 1$ suggests the potential persistence of the infection due to the existence of at least one stationary distribution. Finally, the model is fitted to the actual COVID-19 case data from India during the peak of the second epidemic wave. The insights derived from these projections, particularly regarding the timing of extinction and the magnitude of the infection peak under various scenarios are crucial for public health policymakers for future outbreaks similar to COVID-19.

Keywords Dual vaccine doses · Extinction · Ornstein-Uhlenbeck process · SARS-CoV-2 · Stationary distribution

1 Introduction

COVID-19, a disease resulting from the SARS-CoV-2 virus, was initially identified in Wuhan, China, in December 2019 and has subsequently escalated into a global health crisis [1]. The virus spreads mainly via respiratory droplets and can lead to a variety of symptoms, ranging from discomfort in the respiratory system in a mild manner to illnesses that are threatening like acute respiratory distress syndrome (ARDS) and pneumonia [2]. Beyond the lungs, the impact of SARS-CoV-2 can be on multiple organ systems, leading to cardiovascular, neurological, gastrointestinal issues, and in severe cases, can result in multi-organ failure [3]. Its rapid spread was facilitated by high transmissibility and the presence of asymptomatic carriers, resulting in widespread infections across continents [4].

The pandemic has led to a staggering global impact, with approximately 676 million confirmed infections and 6 million deaths by the end of 2023, severely

T. A. Midhun · K. Murugesan
Department of Mathematics, National Institute of Technology, Tiruchirappalli, Tamil Nadu, India

S. A. Jose (✉) · A. Jirawattanapanit
Department of Mathematics, Faculty of Education, Phuket Rajabhat University, Phuket, Thailand
e-mail: sayooaby999@gmail.com

Published online: 28 January 2025

impacting healthcare systems and economies worldwide [5]. The economic fallout has included disruptions to global supply chains, widespread job losses and economic contractions [6]. Additionally, the phenomenon known as "long COVID", where individuals continue to experience health issues long after the initial infection has resolved, poses significant challenges for ongoing public health management and recovery efforts [7]. This complex situation underscores the importance of continued research, vaccination campaigns and health intervention plans to manage and reduce the impact of infection.

Due to COVID-19 pandemic, India - like most countries in the world and also has a large, heterogeneous population - also hit in different ways. This has led to extreme health consequences and the healthcare infrastructure and resources had crumpled under the burden of nearly 4.5 million confirmed cases with more than half a million deaths to date [8]. This increase in cases has overwhelmed the health care system, causing extreme shortages of beds, oxygen and essential medications [9]. The pandemic has had a profound impact economically, having severely disrupted hospitality, tourism and manufacturing sectors - the list goes on. Enforced restrictions and lockdowns led to massive job losses, decreased incomes and rising poverty levels, further widening the pre-existing economic divides. Indian government has made some extra efforts in their plan to reduce the effect of the pandemic and to control the spread of virus by launching massive vaccination campaigns. That being said, challenges remain in the form of new variants of the virus and the call for equal access to health and the vaccines.

The COVID-19 vaccination in India was one of the largest and most aspirational COVID-19 vaccination campaign ever seen by the world to vaccinate enormous number of people in different geographical areas. Covishield, a domestic version of AstraZeneca's (a global pharmaceutical industry company) AZD1222 vaccine and Covaxin, an inactivated virus vaccine from Bharat Biotech (a biotechnological firm) have been the mainstays of the campaign. Efficacy of Covishield is about 70%, but can increase with an extended interval between first and second doses, so the dual-dose regimen is critical to strengthen the immunity [10]. On the other hand, Covaxin has about 78% efficacy in phase 3 trials [11], further underscoring the importance of the second dose in augmenting immune response, conferring longer-lasting protection as well as protection against the virus. It is the two-dose vaccination strategy that ensures that people attain protective immunity to prevent or at least alleviate infection and transmission. The Sputnik V vaccine, which has an efficacy of 91.6% after 2 doses, has also been included in India's vaccination drive [12]. The vaccination campaign, however, has done wonders in bringing down the number of severe cases of COVID-19 and deaths, despite some hiccups such as supply chain issues, vaccine hesitancy and new variants coming up. As India continues to navigate the pandemic, the focus remains on increasing vaccine coverage and ensuring that the population receives both doses for maximum protection.

Mathematical modeling plays a crucial role in the effective control of epidemic outbreaks by providing a systematic approach to understanding disease dynamics, predicting potential outbreak scenarios and assessing the impact of various interventions such as vaccination. Various deterministic models of infectious diseases have made substantial contributions to the field [13–19]. These models empower researchers to simulate the spread of diseases, identify critical intervention thresholds and optimize public health strategies accordingly. When it comes to COVID-19, the role of mathematical models has been particularly evident. For instance, Nastasi et al. [20] utilized a time-delayed SIRD and SIRDV model to illustrate how vaccination campaigns in Great Britain and Israel were instrumental in significantly reducing both mortality and infection rates. Similarly, Yang et al. [21] underscored the importance of enhancing vaccine efficacy and combining it with non-pharmaceutical interventions to more effectively control the virus spread. In another study, Diagne et al. [22] emphasized the necessity of achieving a critical vaccination threshold to fully eradicate COVID-19. Moreover, Paul et al. [23] proposed a deterministic model highlighting vaccination as the primary tool for managing the COVID-19 impact. Additionally, Angeli et al. [24] proposed an SAIVR model, which includes asymptomatic and vaccinated compartments to better predict the evolution of the epidemic. Furthermore, Zhai et al. [25] illustrated through an SEIR-type model the critical role of vaccination control in preventing the persistence of the disease. Numerous deterministic studies have examined various aspects of COVID-19 and its repercussions from different perspectives [26–28]. In addition to general analyses, numerous modeling studies have specifically focused on understanding COVID-19 infection dynam-

ics and associated interventions within the Indian context. For instance, Foy et al. [29] demonstrated that prioritizing vaccination for older populations in India resulted in the most significant reduction in COVID-19-related deaths. Similarly, Biswas et al. [30] developed a model to study COVID-19 dynamics and predict trends in India. Their analysis, based on data from two distinct periods-1 March to 24 April 2020 and 25 March to 24 April 2020-estimated the average basic reproduction number and emphasized that implementing safe distancing measures and isolating asymptomatic cases could significantly reduce the outbreak size and peak prevalence. In another study, Samui et al. [31] proposed a novel SAIU model to examine COVID-19 transmission dynamics in India from January to April 2020. This study highlighted the importance of accurate data for reliable predictions and stressed the necessity of developing effective therapeutics or vaccines to combat the pandemic. Furthermore, Ambikapathy and Krishnamurthy [32] forecasted COVID-19 cases across 14 countries, including India, showing that 14 to 21 day and 42 day lockdowns significantly reduced case numbers. However, extending lockdown durations beyond 42 days did not yield additional benefits. Their study also revealed that panic shopping scenarios could lead to exponential transmission, demonstrating the failure of intervention measures under such conditions. Taken together, these studies, along with many others focus on the important role of mathematical modeling in formulating effective public health responses and controlling epidemics, particularly through strategic vaccination efforts, as evidenced by the literature.

The studies on SARS-CoV-2 infection mentioned above have primarily employed deterministic models. Nevertheless, a critical aspect often missed by these models is randomness, which can play a crucial role in shaping the infection dynamics. A range of environmental factors can impact epidemic models, such as relative humidity, precipitation and temperature. For example, the following factors contribute to the stochastic complexity of SARS-CoV-2 epidemic dynamics:

(i) The pervasive uncertainty and variability in public health responses and individual behaviors introduce significant unpredictability. Many individuals, influenced by varying levels of awareness, fear, or misinformation, may not adhere consistently to preventive measures or seek timely testing and treatment. This variability affects the overall count and dynamics of COVID-19 cases within the population on a level that is hard to analyze deterministically.

(ii) The presence of SARS-CoV-2 infection shows notable correlations with environmental conditions, such as rainfall and temperature. Research has demonstrated that viral transmission rates and survival can be influenced by temperature fluctuations. For instance, higher temperatures may affect the stability of the virus and its transmission potential. Studies have found that SARS-CoV-2 survival rates on surfaces and in aerosols can vary with temperature, impacting how the virus spreads in different climates. Hence, when analyzing the COVID-19 spread, it is essential to consider the unpredictable aspect of environmental factors [33].

(iii) Asymptomatic carriers play a significant role in the stochastic nature of COVID-19 transmission. These individuals, although infected, do not show symptoms but actively interact within the community, unknowingly spreading the virus on a large scale. Research has demonstrated that the viral load in asymptomatic individuals is comparable to that of symptomatic cases. This is particularly impactful in large populations like India, where it can contribute to a high degree of stochasticity in the spread of the disease [34].

(iv) Mutations in the virus, particularly in regions like the spike protein, can lead to new variants with changed transmissibility, immune evasion, or increased virulence. Such mutations introduce variability into the spread and severity of the disease, making the trajectory of the epidemic unpredictable [35]. Similarly, differences in antibody response between individuals can affect the response of the immune system, while some individuals may produce smaller or less effective antibodies, making them more susceptible to reinfection or longer viral shedding. The variability in the response of the immune system makes the infection dynamics random due to the fact that a few individuals may remain susceptible to reinfection or have severe disease outcomes [36]. Together, these factors contribute to a highly dynamic and uncertain environment, making it difficult to accurately predict the course of the epidemic.

(iii) The growth and transmission patterns of COVID-19 are inherently unpredictable due to the stochas-

tic nature of human interactions. This unpredictability complicates efforts to forecast the speed and direction of the progression of the epidemic, making it challenging to develop precise predictions.

Tackling the intrinsic randomness in disease dynamics poses a considerable challenge. In order to achieve a more precise illustration of the uncertain characteristics of infectious interactions at different phases of an epidemic, stochastic differential equation (SDE) models can be effectively used [37–41]. By incorporating stochastic elements, these models can better capture the variability in disease spread and improve our understanding of epidemic dynamics. There are several SDE models that demonstrate various dynamical behaviors of the SARS-CoV-2 infection dynamics [42–46]. It is evident that most of these models are linearly influenced by standard Gaussian white noise. For instance, consider an approach where the transmission rate β is influenced linearly by standard Gaussian white noise. Specifically, $\beta(t)$ is perturbed as

$$\beta(t) = \bar{\beta} + \kappa \frac{dW}{dt},$$

where $W(t)$ represents the standard Brownian motion defined on $(\Omega, \mathcal{F}, \{\mathcal{F}_t\}_{t\geq 0}, \mathbb{P})$, a complete probability space equipped with a filtration $\{\mathcal{F}_t\}_{t\geq 0}$ that satisfies the usual conditions. Here, κ denotes the intensity of the stochastic white noise. However, this approach is often impractical in real-world applications. The primary issue from a biological perspective can be outlined as follows: for any time interval $[0, t]$, by defining the time average of $\beta(t)$ as $\langle\beta(t)\rangle$, we can compute:

$$\begin{aligned}\langle\beta(t)\rangle &= \frac{1}{t}\int_0^t \beta(\tau)\, d\tau \\ &= \bar{\beta} + \frac{\kappa W(\tau)}{t} \sim \mathbb{N}\left(\bar{\beta}, \frac{\kappa^2}{t}\right),\end{aligned}$$

where $\mathbb{N}(\cdot, \cdot)$ denotes the one-dimensional Gaussian distribution. Evidently, the variance of the average state $\langle\beta(t)\rangle$ over $[0, t]$ is given by $\frac{\kappa^2}{t}$, which diverges to infinity as $t \to 0^+$. This implies that the fluctuations in $\beta(t)$ become excessively large over very small time intervals, a result that is biologically implausible.

Alternatively, natural processes in social and biological systems often display an initial phase of fluctuation before stabilizing around a specific point, a state referred to as homeostasis [47]. For instance, the following examples illustrate this concept:

(i) The immune system adapts to the presence of a pathogen during an epidemic, often producing an initial response followed by immunological memory. Immune responses typically exhibit homeostasis, balancing the need for a strong defense with the risk of overreaction (such as cytokine storms). Lipsitch et al. [48] analyzed the response of the immune system to infectious agents, particularly during epidemics. They demonstrate the homeostatic nature of immune system dynamics by modeling the development of immune responses and their stabilizing effects, focusing on how immunological memory and adaptive responses maintain equilibrium and protect against reinfection.

(ii) Korber et al. [49] studied the D614G mutation in the spike protein of SARS-CoV-2. The authors show that this mutation enhanced the ability of the virus to infect human cells and spread more effectively. They examine the homeostasis-like behavior of viral evolution, where the virus maintains its capacity to spread and infect others while adapting to selective pressures such as immune responses and treatment interventions. The ability of the virus to preserve these characteristics as it evolves suggests a balance between the virus and the immune responses of the host.

Similar behavior can be observed at various stages of infection dynamics beyond the examples provided. In infectious disease modeling, transmission rates and infection levels fluctuate due to stochastic factors like contact patterns and environmental conditions, as previously mentioned. However, these rates often stabilize over time due to factors such as herd immunity or seasonal variations. Allen [50] explores the integration of Ornstein-Uhlenbeck (O-U) processes into epidemiological models to capture the variability in infection rates while accounting for stabilizing factors like vaccination and natural immunity. The author emphasizes how this approach helps model the inherent randomness in epidemic dynamics. Unlike the Gaussian white noise model, which lacks inherent stability [51], the O-U process uniquely combines Gaussian, Markov and stationary characteristics, as first demonstrated by Ornstein and Uhlenbeck in 1930 [52]. Allen [53] further highlighted that the O-U process better accounts for environmental variability compared to linear models driven by white noise, offering characteristics such as

non-negativity, continuity and easier fitting of parameters. Additionally, Gaussian white noise can be viewed as a special case of the O-U process, making the incorporation of the O-U process into models a significant improvement over relying solely on Gaussian white noise. The existing literature contains numerous models that employ the mean-reverting logarithmic O-U process [54–58]. For those interested in further exploration, these references and the studies they cite provide valuable insights into the applications and dynamics of this process.

1.1 Model formulation

In this section, a model is developed that specifically accounts for the dual-dose vaccination strategy, suitable to the epidemiological context of India both in deterministic and stochastic environments. The role of vaccination in dual doses in controlling the COVID-19 spread cannot be overstated, as it has been proven to significantly enhance immunity and reduce the severity of the disease. In India, the dual-dose vaccination strategy was a cornerstone of the national COVID-19 vaccination campaign, starting in January 2021 with the introduction of vaccines like Covishield and Covaxin [59]. This approach aimed to provide broad and sustained immunity across the population, particularly given the large and diverse demographics of the country. Several studies have demonstrated that two doses of COVID-19 vaccines provide greater protection than a single dose, highlighting the critical role of completing the vaccination schedule. In the context of modeling SARS-CoV-2 infection dynamics, incorporating dual doses into compartmental models allows for a more accurate representation of the immunity landscape of the population.

1.1.1 Deterministic model

Assuming homogeneous mixing within the population, where each individual has an equal probability of contact with others, we can use a deterministic compartmental modeling approach to describe the transmission dynamics of the infection. The total population $N(t)$ is categorized based on the disease status of the individual: COVID-19 Susceptible $S(t)$, COVID-19 first dose vaccinated $V_{(i)}(t)$, COVID-19 second dose vaccinated $V_{(ii)}(t)$, COVID-19 exposed $E(t)$, COVID-19 infected $I(t)$ and COVID-19 recovered $R(t)$. The overall population size is expressed as

$$N(t) = S(t) + V_{(i)}(t)+V_{(ii)}(t)+E(t)+I(t)+R(t).$$

Since the availability of COVID-19 vaccination is an important factor, our model includes specific compartments for individuals who have received one or both doses of the vaccine. The transition dynamics between compartments are as follows:

(i) Λ represents the rate at which individuals enter the total population, such as through births or immigration. Among the recruited individuals, a portion will be already vaccinated with the first dose of the COVID-19 vaccine. This fraction is denoted by $\epsilon_1\Lambda$, and these individuals will be assigned to the first-dose vaccinated class. Similarly, another portion of the newly recruited individuals would have received both doses of the COVID-19 vaccine already, represented by the fraction $\epsilon_2\Lambda$. The remaining newly recruited individuals, who are not vaccinated with any doses of the COVID-19 vaccine, are represented by the fraction $(1-\epsilon_1-\epsilon_2)\Lambda$. These individuals will be directly recruited into the susceptible class.

(ii) All individuals have a common natural mortality rate μ.

(iii) Since the COVID-19 vaccine is assumed to be imperfect (i.e., it does not provide complete immunity against infection), vaccinated individuals can still acquire the infection through contact with infected individuals. To account for this, the effective contact rate β (bilinear incidence) is adjusted by a scaling factor $(1-\eta_1)$ and $(1-\eta_2)$ for the first dose vaccinated and second dose vaccinated individuals respectively where the parameter η_1 and η_2 (with $0 \leq \eta_1, \eta_2 \leq 1$) represents the efficacy of the corresponding doses of vaccine. Specifically:

- If $\eta_1 = 1$ or $\eta_2 = 1$, the vaccine provides 100% protection, meaning vaccinated individuals are fully immune to infection, and the effective contact rate for these individuals is reduced to zero.
- Conversely, if $\eta_1 = 0$ or $\eta_2 = 0$, the vaccine offers no protection at all, and vaccinated individuals are just as susceptible to infection as unvaccinated individuals, with the effective contact rate remaining unchanged at β.

This scaling factor $(1-\eta_1)$ and $(1-\eta_2)$ thus captures the reduction in susceptibility of vaccinated individuals relative to unvaccinated individuals. As a result, the infection dynamics reflect the imperfect nature of vaccine-induced immunity, ensuring that vaccinated individuals are still considered within the transmission process, albeit with a reduced likelihood of acquiring the infection.

(iv) The susceptible individuals are vaccinated with the first dose at the rate θ_1 and are further vaccinated with the second dose at the rate θ_2.

(v) Exposed individuals transition to the infected class at a rate ϕ. Also, at a rate τ, some of the exposed individuals can naturally build immunity against the infection and become recovered.

(vi) λ is assumed to be the rate of recovery of infected individuals. Also, infected individuals die due to COVID-19 at a rate ω. Individuals who have completed the two-dose regime of the vaccination gain immunity and move to the recovered class at the rate ρ.

This model framework integrates vaccination effects, disease progression and vital dynamics, offering a detailed approach to analyzing the spread of SARS-CoV-2 within the population. Based on these assumptions, we derive the following non-linear system of ordinary differential equations (ODE) to describe the SARS-CoV-2 infection dynamics:

$$\begin{aligned}
\frac{dS}{dt} &= (1-\epsilon_1-\epsilon_2)\Lambda - \beta SI - (\theta_1+\mu)S,\\
\frac{dV_{(i)}}{dt} &= \epsilon_1\Lambda + \theta_1 S\\
&\quad - (1-\eta_1)\beta V_{(i)}I - (\theta_2+\mu)V_{(i)},\\
\frac{dV_{(ii)}}{dt} &= \epsilon_2\Lambda + \theta_2 V_{(i)}\\
&\quad - (1-\eta_2)\beta V_{(ii)}I - (\rho+\mu)V_{(ii)},\\
\frac{dE}{dt} &= \beta SI + (1-\eta_1)\beta V_{(i)}I\\
&\quad + (1-\eta_2)\beta V_{(ii)}I - (\phi+\tau+\mu)E,\\
\frac{dI}{dt} &= \phi E - (\lambda+\omega+\mu)I,\\
\frac{dR}{dt} &= \rho V_{(ii)} + \tau E + \lambda I - \mu R,
\end{aligned} \tag{1}$$

with initial conditions $S(0) > 0$, $V_{(i)}(0) \geq 0$, $V_{(ii)}(0) \geq 0$, $E(0) \geq 0$, $I(0) \geq 0$ and $R(0) \geq 0$. The compartmental flow diagram of the model (1) is demonstrated in Fig. 1. The parameters along with their description is demonstrated in Table 1.

1.1.2 Stochastic model

In this section, the deterministic model is extended by integrating a stochastic framework using the mean-reverting O-U process. As mentioned earlier, the O-U process is particularly well-suited for capturing the stochastic elements influencing disease dynamics. This approach is especially relevant in the context of diverse demographic and climatic conditions of India. The mean-reverting O-U process allows us to model fluctuations around a long-term average, which is crucial for accurately reflecting the variability and uncertainty inherent in real-world disease transmission. By incorporating this stochastic component, we aim to provide a more robust and realistic representation of how random factors impact the spread of infectious diseases, addressing the complex and unpredictable nature of the epidemic in varying environmental and population settings.

Building on the work of Allen [53], this study introduces a stochastic component to the SARS-CoV-2 transmission rate β by modeling it with the O-U process. Specifically, we consider the logarithm of $\beta(t)$ to evolve according to the following SDE:

$$d\log\beta(t) = \kappa_1(\log\bar{\beta} - \log\beta(t))dt + \kappa_2 dW(t), \tag{2}$$

where κ_1 denotes the speed of mean reversion, κ_2 represents the volatility of the noise, $\log\bar{\beta}$ is the long-term mean value of $\log\beta(t)$. Furthermore, let $(\Omega, \mathcal{F}, \{\mathcal{F}_t\}_{t\geq 0}, \mathbb{P})$ be a complete probability space with a filtration $\{\mathcal{F}_t\}_{t\geq 0}$ satisfying the usual conditions and $W(t)$ is the standard Brownian motion defined on it. Here, the logarithm of $\beta(t)$ is used to ensure that the transmission rate remains non-negative, even in the presence of stochastic noise. Now, we can easily verify that the system (2) has a unique exact solution given by:

$$\log\beta(t) = \log\bar{\beta} + \big(\log\beta(0) - \log\bar{\beta}\big)\exp(-\kappa_1 t) + \kappa_2\int_0^t \exp(-\kappa_1(t-s))dW(s).$$

Additionally, we observe the following:

$$\log\beta(t) \sim \mathbb{N}\Big(\log\bar{\beta} + \big(\log\beta(0) - \log\bar{\beta}\big)\exp(-\kappa_1 t), \frac{\kappa_2^2(1-\exp(-2\kappa_1 t))}{2\kappa_1}\Big),$$

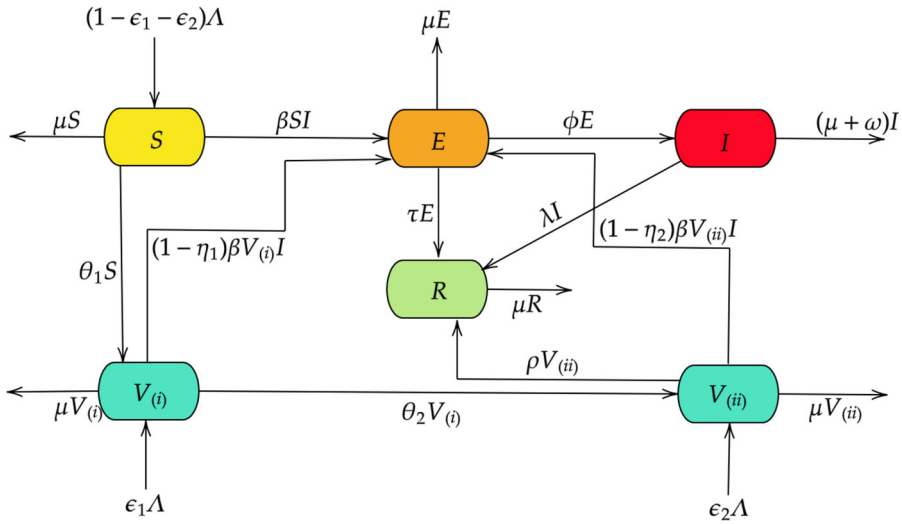

Fig. 1 Flow diagram illustrating the epidemiological model (1), depicting the interactions between the compartments along with key model parameters and their influence on disease dynamics

Table 1 Overview of model parameters influencing the dynamics of the disease

Parameters	Description
Λ	Rate of recruitment into the population
β	COVID-19 transmission rate
μ	Rate of natural mortality
ω	COVID-19 induced death rate
θ_1	Rate of COVID-19 first dose vaccination
θ_2	Rate of COVID-19 second dose vaccination
η_1	COVID-19 first dose vaccine efficacy
η_2	COVID-19 second dose vaccine efficacy
ϕ	Rate of progression from exposed to infected
λ	Rate of recovery of infected individuals
τ	Rate of recovery of of exposed individuals
ρ	Rate of developing immunity through vaccination
ϵ_1	Proportion of individuals newly recruited and receiving their first vaccine dose
ϵ_2	Proportion of individuals newly recruited and receiving their second vaccine dose

$$\lim_{t\to 0^+} \mathbb{E}\left(\log\beta(t)\right) = \log\beta(0),$$
$$\lim_{t\to 0^+} \mathrm{Var}\left(\log\beta(t)\right) = 0,$$
$$\lim_{t\to \infty} \mathbb{E}\left(\log\beta(t)\right) = \log\bar{\beta},$$
$$\lim_{t\to \infty} \mathrm{Var}\left(\log\beta(t)\right) = \frac{\kappa_2^2}{2\kappa_1}.$$

Moreover, if we denote $\langle\log\beta(t)\rangle$ as the time average of $\log\beta(t)$ over the interval $[0, t]$, then we have:

$$\mathrm{Var}\left(\langle\log\beta(t)\rangle\right) = \frac{\kappa_2^2}{3}t + \mathrm{O}(t^2).$$

This implies that the variations in $\log\beta(t)$ will remain small over short time intervals, which aligns with the typical behavior observed in most epidemic systems, thereby addressing one of the main limitations of the linear Gaussian white noise modeling. Therefore, this process is a valid way to model the random effects of key parameters, both biologically and mathematically. Now, for the ease of writing, let us denote

$$b(t) = \log\beta(t) - \log\bar{\beta}.$$

Subsequently, the stochastic counterpart of the deterministc model (1) incorporating logarithmic mean-

reverting O-U process is formulated as follows:

$$\begin{aligned}
db(t) &= -\kappa_1 b(t) + \kappa_2 dW(t),\\
dS(t) &= \big[(1-\epsilon_1-\epsilon_2)\Lambda - \bar{\beta}\\
&\quad \exp(b(t))SI - (\theta_1+\mu)S\big]dt,\\
dV_{(i)}(t) &= \big[\epsilon_1\Lambda + \theta_1 S - (1-\eta_1)\bar{\beta}\\
&\quad \exp(b(t))V_{(i)}I - (\theta_2+\mu)V_{(i)}\big]dt,\\
dV_{(ii)}(t) &= \big[\epsilon_2\Lambda + \theta_2 V_{(i)} - (1-\eta_2)\bar{\beta}\\
&\quad \exp(b(t))V_{(ii)}I - (\rho+\mu)V_{(ii)}\big]dt,\\
dE(t) &= \big[\bar{\beta}\exp(b(t))SI + (1-\eta_1)\bar{\beta}\\
&\quad \exp(b(t))V_{(i)}I + (1-\eta_2)\bar{\beta}\\
&\quad \exp(b(t))V_{(ii)}I - (\phi+\tau+\mu)E\big]dt,\\
dI(t) &= [\phi E - (\lambda+\omega+\mu)I]\,dt,\\
dR(t) &= \big[\rho V_{(ii)} + \tau E + \lambda I - \mu R\big]dt.
\end{aligned} \tag{3}$$

This stochastic framework enables a more realistic representation of dynamic interactions in the system by accounting for random fluctuations in transmission rates. To our knowledge, no existing stochastic model for SARS-CoV-2 infection with dual vaccine doses using Indian data incorporates the logarithmic mean-reverting O-U process. This gap highlights the novelty and importance of our research, which introduces a new approach to understanding the stochastic dynamics of SARS-CoV-2 transmission by integrating environmental variability and vaccine effects. This study presents the following key contributions and innovations:

(i) This study begins with the construction of a deterministic model and subsequently incorporates the logarithmic mean-reverting O-U process to develop a stochastic counterpart. This model examines the transmission dynamics of SARS-CoV-2, accounting for the effects of dual vaccine doses. The approach captures random fluctuations more accurately than linear white noise perturbations, leading to a model that better represents real-world dynamics.

(ii) We thoroughly analyze the deterministic model, establishing the existence and uniqueness of a global positive solution that remains bounded. Additionally, we derive the basic reproduction number R_0^d and assess the local asymptotic stability of the disease-free equilibrium, particularly when $R_0^d < 1$.

(iii) An extensive analysis of the stochastic model yields two crucial threshold parameters, R_0^e and R_0^s. These parameters are key to determining whether the infection will decline or persist in the population. Specifically, the infection will exponentially decrease when $R_0^e < 1$, while the presence of at least one stationary distribution $\pi(\cdot)$ for $R_0^s > 1$ indicates that the infection is likely to persist in the long term.

(iv) We calibrate the stochastic model using actual COVID-19 case data from India during the emergence till the peak of the second wave, from February 28 to May 02, 2021. This calibration enables the derivation of parameter values suited to the specific context. By conducting numerical simulations with these parameters, we validate our theoretical findings and project potential outcomes under various scenarios.

(v) The sensitivity analysis of the model parameters was conducted using a combined approach of Latin Hypercube Sampling (LHS) and Partial Rank Correlation Coefficient (PRCC) methods. This analysis enabled various projections of the model, with a particular focus on the extinction time and the peak size of the COVID-19 epidemic wave. These projections provide valuable insights for public health policymakers, supporting more effective strategies for controlling and managing future COVID-19 outbreaks.

The rest of the article is structured as follows: Sect. 2 lays the groundwork by presenting fundamental concepts and key lemmas to aid comprehension. Moving forward, Sect. 3 examines the uniqueness and existence of a global positive solution for the deterministic model (1) which is bounded, including the derivation of the basic reproduction number R_0^d. Also, in this section we derive the criteria for local asymptotic stability. In Sect. 4, we explore the criteria for the existence of a stationary distribution of the stochastic model (3) through the introduction of the threshold parameter R_0^s and determine the conditions for exponential extinction of the infection using another threshold parameter R_0^e. Section 5 then applies our stochastic model to empirical data from India, validates the theoretical findings with numerical simulations, and provides insights based on model projections. Lastly, Sect. 6 summarizes the main findings and offers concluding remarks.

2 Preliminaries

In this section, we establish key results that are essential for analyzing the complex dynamic behaviors of the system given in model (3). To facilitate our discussion throughout this paper, we introduce the following notations:

- $\mathbb{R}^k_+$ denotes the set of vectors $v = (v_1, v_2, \ldots, v_k) \in \mathbb{R}^k$ where $v_i > 0$ for each $i = 1, 2, 3, \ldots, k$.
- $\bar{\mathbb{R}}^k_+$ represents the set of vectors $v = (v_1, v_2, \ldots, v_k) \in \mathbb{R}^k$ with $v_i \geq 0$ for all $i = 1, 2, 3, \ldots, k$.
- $C^{2,1}(\mathbb{R}^k \times \mathbb{R}_+; \bar{\mathbb{R}}_+)$ is the class of non-negative functions $U(Z, t)$ defined on $\mathbb{R}^k \times \mathbb{R}_+$ that are twice continuously differentiable with respect to Z and once with respect to t.
- $\mathbb{I}_G$ denotes the indicator function for the set G.
- B^{-1} denotes the inverse of an invertible matrix B. For a square matrix B, $|B|$ represents its determinant.
- For any real numbers b_i $(i = 1, 2, 3, \ldots, n)$, $\text{diag}(b_1, b_2, \ldots, b_n)$ denotes an n-order diagonal matrix.

We now introduce some fundamental concepts related to stochastic differential equations (for a detailed understanding, refer to [60]). Consider a k-dimensional stochastic process $Z(t)$ for $t \geq 0$, governed by the following stochastic differential equation:

$$dZ(t) = g(Z(t), t)\, dt + h(Z(t), t)\, dW(t), \tag{4}$$

where $g \in L^1(\mathbb{R}_+; \mathbb{R}^k)$, $h \in L^2(\mathbb{R}_+; \mathbb{R}^{k\times m})$, and $W(t) = (W_t^1, W_t^2, \ldots, W_t^k)$ represents a k-dimensional Brownian motion defined on the complete probability space $(\Omega, \mathcal{F}, \{\mathcal{F}_t\}_{t\geq 0}, \mathbb{P})$ with the filtration $\{\mathcal{F}_t\}_{t\geq 0}$ satisfying the usual conditions. Define the following operator of differentiation $\mathcal{L}$:

$$\mathcal{L} = \frac{\partial}{\partial t} + \sum_{i=1}^{k} g_i(Z(t), t) \frac{\partial}{\partial Z_i} + \frac{1}{2} \sum_{i,j=1}^{k} \left[h^T(Z(t), t) h(Z(t), t) \right]_{ij} \frac{\partial^2}{\partial Z_i \partial Z_j}.$$

When $\mathcal{L}$ acts on a function $U \in C^{2,1}(\mathbb{R}^k \times \mathbb{R}_+; \bar{\mathbb{R}}_+)$, we get

$$\mathcal{L}U(Z(t), t) = U_t(Z(t), t) + U_Z(Z(t), t) g(Z(t), t) + \frac{1}{2} \text{trace} \left[h^T(Z(t), t) U_{ZZ} h(Z(t), t) \right],$$

where $U_t = \frac{\partial U}{\partial t}$, $U_Z = \left(\frac{\partial U}{\partial Z_1}, \ldots, \frac{\partial U}{\partial Z_k} \right)$, and $U_{ZZ} = \left(\frac{\partial^2 U}{\partial Z_i \partial Z_j} \right)_{k\times k}$. The following lemmas will support the further analysis of the model (3).

Lemma 1 (Young's Inequality) *For any sufficiently small $\epsilon > 0$, the following inequality holds:*

$$\beta \leq \epsilon \beta^2 + \frac{1}{4\epsilon}.$$

Lemma 2 *For the stochastic differential equation*

$$db(t) = -\kappa_1 b(t)\, dt + \kappa_2\, dW(t),$$

where κ_1 and κ_2 are positive constants and $W(t)$ denotes standard Brownian motion, the following results hold:

(i)

$$\lim_{t\to\infty} \frac{1}{t} \int_0^t |\exp(b(s)) - 1|\, ds \leq \left(1 + \exp\left(\frac{\kappa_2^2}{\kappa_1} \right) - 2\exp\left(\frac{\kappa_2^2}{4\kappa_1} \right) \right)^{\frac{1}{2}}.$$

(ii) *For $r > 0$,*

$$\lim_{t\to\infty} \frac{1}{t} \int_0^t \exp(rb(s))\, ds = \exp\left(\frac{r^2\kappa_2^2}{4\kappa_1} \right).$$

Lemma 3 [61] *Consider a bounded closed domain $\mathbb{D} \subset \mathbb{R}^k$ with a regular boundary $\partial\mathbb{D}$. For any initial value $Y(0) \in \mathbb{R}^k$, if the following condition holds:*

$$\liminf_{t\to\infty} \frac{1}{t} \int_0^t \mathbb{P}(s, Y(s), \mathbb{D})\, ds > 0 \quad a.s.,$$

where $\mathbb{P}(s, Y(s), \cdot)$ denotes the transition probability of $Y(t)$, then the system described by (4) will have a solution with the Feller property. Moreover, the system (4) will have at least one invariant probability measure $\pi(\cdot)$ defined on $\mathbb{R}^k$, indicating the existence of at least one stationary distribution $\pi(\cdot)$ on $\mathbb{R}^k$.

3 Deterministic model analysis

In this section, we rigorously validate the deterministic model by proving existence, uniqueness, positivity and boundedness of the solution. We also derive the basic reproduction number and analyze the stability of the disease-free equilibrium, offering insights into the conditions for potential eradication. These results lay the groundwork for incorporating stochastic elements into the model.

3.1 Existence and uniqueness of global positive solution

It is crucial to ensure that the model (1) is both mathematically sound and biologically accurate under all relevant conditions, aligning its predictions with real-world dynamics. In this direction, the existence and uniqueness of the global positive solution of the model (1) is proved. To accomplish this, we define the function g as follows:

$$g\begin{pmatrix} S \\ V_{(i)} \\ V_{(ii)} \\ E \\ I \\ R \end{pmatrix} = \begin{pmatrix} (1-\epsilon_1-\epsilon_2)\Lambda - \beta SI - (\theta_1+\mu)S, \\ \epsilon_1\Lambda + \theta_1 S - (1-\eta_1)\beta V_{(i)} I - (\theta_2+\mu)V_{(i)}, \\ \epsilon_2\Lambda + \theta_2 V_{(i)} - (1-\eta_2)\beta V_{(ii)} I - (\rho+\mu)V_{(ii)}, \\ \beta SI + (1-\eta_1)\beta V_{(i)} I + (1-\eta_2)\beta V_{(ii)} I - (\phi+\tau+\mu)E, \\ \phi E - (\lambda+\omega+\mu)I, \\ \rho V_{(ii)} + \tau E + \lambda I - \mu R \end{pmatrix}.$$

The function g is continuously differentiable on $\mathbb{R}^6_+$, and it is locally Lipschitz on any bounded subset of $\mathbb{R}^6_+$. These properties ensure the existence and uniqueness of a maximal solution for the system (1). However, the positivity and boundedness of the solution, which are critical for the practical relevance of any epidemiological model, are not yet guaranteed. The following theorem will address this aspect:

Theorem 3.1 *Let $S(0) > 0$, $V_{(i)}(0) > 0$, $V_{(ii)}(0) > 0$, $E(0) > 0$, $I(0) >$ and $R(0) > 0$ be the initial values for the model (1). Then the domain $\mathbb{R}^6_+$ is an invariant domain for the model (1).*

Proof The goal is to prove that the tangent vector of the system points towards the positive orthant at the boundary of $\mathbb{R}^6_+$. We can observe that

$$\begin{aligned} \left.\frac{dS}{dt}\right|_{S=0} &= (1-\epsilon_1-\epsilon_2)\Lambda > 0, \\ \left.\frac{dV_{(i)}}{dt}\right|_{V_{(i)}=0} &= \epsilon_1\Lambda + \theta_1 S > 0, \\ \left.\frac{dV_{(ii)}}{dt}\right|_{V_{(ii)}=0} &= \epsilon_2\Lambda + \theta_2 V_{(i)} > 0, \\ \left.\frac{dE}{dt}\right|_{E=0} &= \beta SI + (1-\eta_1)\beta V_{(i)} I \\ &\quad + (1-\eta_2)\beta V_{(ii)} I > 0, \\ \left.\frac{dI}{dt}\right|_{I=0} &= \phi E > 0, \\ \left.\frac{dR}{dt}\right|_{R=0} &= \rho V_{(ii)} + \tau E + \lambda I > 0. \end{aligned}$$

Then by applying Lemma 2 in [62], it can be stated that $\mathbb{R}^+_6$ is an invariant domain for the model (1) with positive initial conditions. This concludes the proof. □

Remark 3.2 Consider the total population as $N(t) = S(t) + V_{(i)}(t) + V_{(ii)}(t) + E(t) + I(t) + R(t)$. Then

$$\frac{dN}{dt} = \Lambda - \mu N - \omega I, \quad \forall t \geq 0,$$

which implies

$$\frac{dN}{dt} \leq \Lambda - \mu N, \quad \forall t \geq 0.$$

This leads to the inequality

$$N(t) \leq \exp(-\mu t)N(0) + \frac{\Lambda}{\mu}\left(1 - \exp(-\mu t)\right), \quad \forall t \geq 0,$$

and further we have

$$N(t) \leq \max\left\{N(0), \frac{\Lambda}{\mu}\right\}, \quad \forall t \geq 0.$$

Thus, the solution is globally defined and bounded on $[0, \infty)$.

3.2 Basic reproduction number

In order to derive the basic reproduction number for the model (1), we utilize the popular next-generation matrix method. For that, the disease free equilibrium point $\Sigma^0 = \left(S^0, V^0_{(i)}, V^0_{(ii)}, E^0, I^0, R^0\right)$ of the model is computed as

$$\begin{aligned} S^0 &= \frac{(1-\epsilon_1-\epsilon_2)\Lambda}{\theta_1+\mu}, \\ V^0_{(i)} &= \frac{\epsilon_1\Lambda + \theta_1 S^0}{\theta_2+\mu}, \\ V^0_{(ii)} &= \frac{\epsilon_2\Lambda + \theta_2 V^0_{(i)}}{\rho+\mu}, \\ E^0 &= 0, \end{aligned}$$

$$I^0 = 0,$$
$$R^0 = \frac{\rho V^0_{(ii)}}{\mu}.$$

Next, at this disease-free equilibrium point Σ^0, we compute the jacobian matrix F for the new infections

$$F = \begin{pmatrix} 0 & \beta S^0 + (1-\eta_1)\beta V^0_{(i)} + (1-\eta_2)\beta V^0_{(ii)} \\ 0 & 0 \end{pmatrix}.$$

Similarly, for the remaining transfer terms also we compute the jacobian matrix V as

$$V = \begin{pmatrix} \phi + \tau + \mu & 0 \\ -\phi & \lambda + \omega + \mu \end{pmatrix}.$$

Now, we find out the spectral radius of the matrix FV^{-1}, which is the basic reproduction number. This is denoted as R^d_0 and it can be seen that

$$R^d_0 = \frac{\phi\left(\beta S^0 + (1-\eta_1)\beta V^0_{(i)} + (1-\eta_2)\beta V^0_{(ii)}\right)}{(\lambda + \omega + \mu)(\phi + \tau + \mu)}.$$

3.3 Local stability of the disease-free equilibrium point

In this subsection, we demonstrate the local asymptotic stability of the disease-free equilibrium. This result is crucial for identifying the conditions that allow for the potential eradication of the virus from the population.

Theorem 3.3 *The disease-free equilibrium point Σ_0 is locally asymptotically stable when $R^d_0 < 1$ and unstable when $R^d_0 > 1$.*

Proof The Jacobian matrix of the model (1) at the disease-free equilibrium point Σ_0 is given by

$$\mathcal{J}(\Sigma_0) = \begin{pmatrix} -(\theta_1+\mu) & 0 & 0 & 0 & -\frac{\beta(1-\epsilon_1-\epsilon_2)\Lambda}{\theta_1+\mu} & 0 \\ \theta_1 & -(\theta_2+\mu) & 0 & 0 & -\frac{(1-\eta_1)\beta(\epsilon_1\Lambda+\theta_1 S^0)}{\theta_2+\mu} & 0 \\ 0 & \theta_2 & -(\rho+\mu) & 0 & -\frac{(1-\eta_2)\beta(\epsilon_2\Lambda+\theta_2 V^0_{(i)})}{\rho+\mu} & 0 \\ 0 & 0 & 0 & -(\phi+\tau+\mu) & \beta(S^0+(1-\eta_1)V^0_{(i)}+(1-\eta_2)V^0_{(ii)}) & 0 \\ 0 & 0 & 0 & \phi & -(\lambda+\omega+\mu) & 0 \\ 0 & 0 & \rho & \tau & \lambda & -\mu \end{pmatrix}.$$

The characteristic roots x_i $(i = 1, 2, \ldots, 6)$ are found to be

$$x_1 = -\mu,$$
$$x_2 = -(\mu + \theta_1),$$
$$x_3 = -(\theta_2 + \mu),$$
$$x_4 = -(\rho + \mu),$$

while x_5 and x_6 are the solutions to the quadratic equation $x^2 + a_1 x + a_2 = 0$, where

$$a_1 = (\lambda + \omega + \mu)(\phi + \tau + \mu) > 0,$$
$$a_2 = (\lambda + \omega + \mu)(\phi + \tau + \mu) - \beta\phi\left(S^0 + (1-\eta_1)V^0_{(i)} + (1-\eta_2)V^0_{(ii)}\right),$$
$$= (\lambda + \omega + \mu)(\phi + \tau + \mu)\left(1 - R^d_0\right).$$

It can be observed that x_1, x_2, x_3 and x_4 are all negative, as all parameters are positive. Additionally, $a_2 > 0$ when $R^d_0 < 1$, which means that the quadratic polynomial satisfies the Routh-Hurwitz criterion, ensuring the local asymptotic stability of the disease-free equilibrium when $R^d_0 < 1$. Conversely, if $R^d_0 > 1$, the disease-free equilibrium is unstable. This completes the proof. □

4 Stochastic model analysis

Transitioning to the stochastic model from the deterministic environment is essential, as it introduces randomness to capture the inherent uncertainties and fluctuations present in real-world SARS-CoV-2 dynamics. By incorporating the O-U process, we can analyze how these stochastic variations influence disease

spread and the effectiveness of intervention strategies. This analysis offers a richer, more nuanced understanding of potential scenarios, allowing us to account for the unpredictable nature of the virus. Ultimately, this deeper insight aids in refining public health strategies, enhancing our ability to manage and mitigate the impact of the virus more effectively. The framework utilized in this section for the analysis of the model (3) is inspired by the research conducted by Shi and Jiang, as presented in their work [63].

4.1 Existence and uniqueness of a global positive solution

This subsection establishes the existence and uniqueness of a global positive solution for the stochastic model (3). This proof is crucial in demonstrating that the system behaves consistently over time, ensuring that the solution remains biologically meaningful by preventing negative or unbounded values. For that, we present the following theorem:

Theorem 4.1 *For any initial value* $X(0) = (S(0), V_{(i)}(0), V_{(ii)}(0), E(0), I(0), b(0)) \in \mathbb{R}^5_+ \times \mathbb{R}$, *there exists a unique solution* $X(t) = (S(t), V_{(i)}(t), V_{(ii)}(t), E(t), I(t), b(t))$ *for* $t \geq 0$, *and the solution remains in* $\mathbb{R}^5_+ \times \mathbb{R}$ *a.s.*

Proof The local Lipschitz continuity of the system (3) can be very easily verified. Therefore, for any initial value $(S(0), V_{(i)}(0), V_{(ii)}(0), E(0), I(0), b(0)) \in \mathbb{R}^5_+ \times \mathbb{R}$, on the interval $[0, \tau_e)$ the existence of a unique maximal local solution $(S(t), V_{(i)}(t), V_{(ii)}(t), E(t), I(t), b(t))$ can be guaranteed. Here, τ_e is known as the explosion time. Now, we prove that this solution is global, i.e., $\tau_e = \infty$ a.s. To this end, let $n_0 \geq 1$ be a sufficiently large integer such that $(S(0), V_{(i)}(0), V_{(ii)}(0), E(0), I(0), b(0))$ will lie within the interval $\left[\frac{1}{n_0}, n_0\right]$. Now, the following sequence of stopping times can be defined for every integer $n \geq n_0$:

$$\tau_n = \left\{ t \in [0, \tau_e) : \begin{array}{c} \min\left(S(t), V_{(i)}(t), V_{(ii)}(t), E(t), I(t), \exp(b(t))\right) \leq \frac{1}{n} \\ \text{(or)} \\ \max\left(S(t), V_{(i)}(t), V_{(ii)}(t), E(t), I(t), \exp(b(t))\right) \geq n \end{array} \right\}$$

Throughout this article, we establish that $\inf \phi = \infty$ a.s. (usually, ϕ denotes the empty set). It is evident that as n approaches ∞, τ_n is monotonically increasing. Let $\tau_\infty = \lim_{n\to\infty} \tau_n$. Consequently, $\tau_\infty \leq \tau_n$ a.s. If $\tau_\infty = \infty$ a.s. holds true, then it follows that $\tau_e = \infty$ a.s. Additionally, $(S(t), V_{(i)}(t), V_{(ii)}(t), E(t), I(t), \exp(b(t))) \in \mathbb{R}^5_+ \times \mathbb{R}$ a.s $\forall t \geq 0$. To complete the proof, we aim to establish that $\tau_\infty = \infty$ a.s. To do so, let us assume the opposite. This implies that $\mathbb{P}\{\tau_\infty \leq T\} > \epsilon$, for some constants $T > 0$ and $\epsilon \in (0, 1)$. Consequently, there exists an integer $n_1 \geq n_0$ such that $\mathbb{P}\{\tau_n \leq T\} > \epsilon$ for all $n \geq n_1$. For any $(S(t), V_{(i)}(t), V_{(ii)}(t), E(t), I(t), \exp(b(t))) \in \mathbb{R}^5_+ \times \mathbb{R}$, we define a non-negative C^2-function U_1 as follows:

$$\begin{aligned} &U_1(S, V_{(i)}, V_{(ii)}, E, I, b) \\ &\quad = (\exp(b) - b - 1) + (S - 1 - \log S) \\ &\qquad + \left(V_{(i)} - 1 - \log V_{(i)}\right) \\ &\qquad + \left(V_{(ii)} - 1 - \log V_{(ii)}\right) \\ &\qquad + (E - 1 - \log E) + (I - 1 - \log I). \end{aligned}$$

The non-negativity of U_1 can be obtained through the inequality $y - 1 - \log y \geq 0$ for $y > 0$. Now, by utilizing the Itô's formula, we get

$$\begin{aligned} \mathcal{L}U_1 = &-\kappa_1 b(\exp(b) - 1) + \frac{\kappa_2^2 \exp(b)}{2} \\ &+ \left(1 - \frac{1}{S}\right)((1 - \epsilon_1 - \epsilon_2)\Lambda \\ &- \bar{\beta}\exp(b(t))SI - (\theta_1 + \mu)S\Big) \\ &+ \left(1 - \frac{1}{V_{(i)}}\right)(\epsilon_1\Lambda + \theta_1 S \\ &- (1 - \eta_1)\bar{\beta}\exp(b(t))V_{(i)}I - (\theta_2 + \mu)V_{(i)}\Big) \\ &+ \left(1 - \frac{1}{V_{(ii)}}\right)\left(\epsilon_2\Lambda + \theta_2 V_{(i)}\right. \\ &- (1 - \eta_2)\bar{\beta}\exp(b(t))V_{(ii)}I - (\rho + \mu)V_{(ii)}\Big) \end{aligned}$$

$$
\begin{aligned}
&+\left(1-\frac{1}{E}\right)\left(\bar{\beta}\exp(b(t))SI+(1-\eta_1)\bar{\beta}\right.\\
&\exp(b(t))V_{(i)}I+(1-\eta_2)\bar{\beta}\\
&\left.\exp(b(t))V_{(ii)}I-(\phi+\tau+\mu)E\right)\\
&+\left(1-\frac{1}{I}\right)(\phi E-(\lambda+\omega+\mu)I),\\
&\leq -\kappa_1 b\left(\exp(b)-1\right)+\frac{\kappa_2^2\exp(b)}{2}+\bar{\beta}\\
&\exp(b)(1-\eta_1-\eta_2)+\Lambda+\theta_1+\theta_2+\phi\\
&+\tau+\lambda+\omega+\rho+5\mu.
\end{aligned}
$$

Now, let us take $A(t)=S(t)+V_{(i)}(t)+V_{(ii)}(t)+E(t)+I(t)$. Then, we can note that

$$A\leq\Lambda-\mu A,$$

which implies

$$A(t)\leq\Delta=\begin{cases}\dfrac{\Lambda}{\mu}, & \text{if}\quad A(0)\leq\dfrac{\Lambda}{\mu}\\ A(0), & \text{if}\quad A(0)>\dfrac{\Lambda}{\mu}\end{cases}.$$

Also let us denote

$$
\begin{aligned}
g(b)=&-\kappa_1 b\left(\exp(b)-1\right)+\frac{\kappa_2\exp(b)}{2}\\
&+\bar{\beta}\exp(b)(1-\eta_1-\eta_2).
\end{aligned}
$$

It can be noted that $g(b)\to-\infty$ as $|b|\to\infty$. Therefore, $g(b)$ always has an upper bound. Now, let

$$\sup_{b\in\mathbb{R}}\{g(b)\}=C_1<\infty.$$

Then, we have

$$
\begin{aligned}
\mathcal{L}W_1\leq\ & C_1+\Lambda+\theta_1+\theta_2+\phi\\
&+\tau+\lambda+\omega+\rho+5\mu\leq C_2,
\end{aligned}
$$

where a well-defined positive constant C_2 can be easily established. This completes the proof. □

Remark 4.2 From the model (3), it follows that

$$dA<\Lambda-\mu A.$$

Moreover,

$$A(t)<\frac{\Lambda}{\mu}+\exp(-\mu t)\left[A(0)-\frac{\Lambda}{\mu}\right].$$

Thus, if $A(0)<\dfrac{\Lambda}{\mu}$, then $A(t)<\dfrac{\Lambda}{\mu}$ almost surely. Further, we can observe

$$dS<(1-\epsilon_1-\epsilon_2)\Lambda-(\theta_1+\mu)S.$$

Therefore,

$$S(t)<S^0+\exp\left(-(\theta_1+\mu)t\right)(S(0)-S^0).$$

We further observe that if $S(0)<S^0$, then $S(t)<S^0$. Additionally

$$dV_{(i)}<\epsilon_1\Lambda+\theta_1 S^0-(\theta_2+\mu)V_{(i)},$$

implies

$$V_{(i)}(t)<V_{(i)}^0+\exp\left(-(\theta_2+\mu)t\right)(V_{(i)}(0)-V_{(i)}^0).$$

Furthermore, if $V_{(i)}(0)<V_{(i)}^0$, then $V_{(i)}(t)<V_{(i)}^0$ almost surely. Similarly, considering

$$dV_{(ii)}<\epsilon_2\Lambda+\theta_2 V_{(i)}^0-(\rho+\mu)V_{(ii)},$$

we obtain

$$V_{(ii)}(t)<V_{(ii)}^0+\exp\left(-(\rho+\mu)t\right)(V_{(ii)}(0)-V_{(ii)}^0).$$

Also, if $V_{(ii)}(0)<V_{(ii)}^0$, then $V_{(ii)}(t)<V_{(ii)}^0$ almost surely. Hence, we can define the following positive invariant region:

$$
\begin{aligned}
\Theta=\Big\{&(b,S,V_{(i)},V_{(ii)},E,I)\in\mathbb{R}_+^5\times\mathbb{R}:\\
&S<S^0,V_{(i)}<V_{(i)}^0,V_{(ii)}<V_{(ii)}^0,A<\frac{\Lambda}{\mu}\Big\}.
\end{aligned}
$$

Hereafter, we take $X(0)\in\Theta$ always. □

4.2 Existence of stationary distribution of the model (3)

In this subsection, we establish the existence of a stationary solution for the stochastic model (3). The stationary solution represents a stable long-term behavior of the system, where the effects of random fluctuations are balanced over time. To explore this, we introduce a stochastic threshold R_0^s, defined as:

$$R_0^s=\frac{\bar{\beta}\phi\left\{S^0\exp\left(\frac{\kappa_2^2}{16\kappa_1}\right)+(1-\eta_2)V_{(i)}^0\exp\left(\frac{\kappa_2^2}{12\kappa_1}\right)+(1-\eta_2)V_{(ii)}^0\exp\left(\frac{\kappa_2^2}{12\kappa_1}\right)\right\}}{(\lambda+\omega+\mu)(\phi+\tau+\mu)}.$$

This expression quantifies the average transmission potential of the virus within the stochastic framework, considering the natural randomness. Now, consider the following theorem:

Theorem 4.3 *If $R_0^s > 1$, the solution of the stochastic model (3) admits atleast one stationary distribution.*

Proof The proof outline can be segmented into three main steps. Initially, we construct a non-negative C^2-function denoted as $U_2(S, V_{(i)}, V_{(ii)}, E, I, b)$. Subsequently, we select a compact set $\mathbb{D} \subset \Theta$ such that $\mathcal{L}U_2 \leq -1$ for all $(S, V_{(i)}, V_{(ii)}, E, I, b) \in \Theta \backslash \mathbb{D}$. The final step is to establish the existence of a stationary distribution.

Step 1 (Construction of a non-negative $\mathbf{C^2}$-function): Let us first consider the function Y_1 defined as

$$Y_1 = -c_1 \log S - \log V_{(i)} + c_2 V_{(i)},$$

where c_1 and c_2 will be defined on a subsequent stage of this proof. Now, we apply the Itô's formula

$$\begin{aligned}
\mathcal{L}Y_1 \leq & -\frac{\epsilon_1 \Lambda}{V_{(i)}} - \frac{\theta_1 S}{V_{(i)}} + (1-\eta_1)\bar{\beta} I \\
& \exp\left(b(t)\right) + \theta_2 + \mu - \frac{c_1(1-\epsilon_1-\epsilon_2)\Lambda}{S} \\
& + c_1 \bar{\beta} \exp\left(b(t)\right) I + c_1\theta_1 + c_1\mu \\
& + c_2(\epsilon_1\Lambda + \theta_1 S) - c_2(\theta_2+\mu)V_{(i)}, \\
\leq & -\frac{\epsilon_1 \Lambda}{V_{(i)}} - \frac{\theta_1 S}{V_{(i)}} \\
& - \frac{c_1(1-\epsilon_1-\epsilon_2)\Lambda}{S} - c_2(\theta_2+\mu)V_{(i)} \\
& + (1-\eta_1)\bar{\beta} I \exp(b(t)) \\
& + \theta_2 + \mu + c_1(\bar{\beta} I \exp(b(t)) + \theta_1 + \mu) \\
& + c_2(\epsilon_1\Lambda + \theta_1 S^0), \\
\leq & -\frac{\epsilon_1 \Lambda}{V_{(i)}} - 3\left\{\theta_1 c_1 c_2 (1-\epsilon_1-\epsilon_2)(\theta_2+\mu)\Lambda\right\}^{\frac{1}{3}} \\
& + (1-\eta_1)\bar{\beta} I \exp(b(t)) + \theta_2 + \mu \\
& + c_1(\bar{\beta} I \exp(b(t)) + \theta_1 + \mu) + c_2(\epsilon_1\Lambda + \theta_1 S^0).
\end{aligned}$$

Now, we can choose c_1 and c_2 to be

$$\begin{aligned}
c_1(\theta_1+\mu) &= c_2(\epsilon_1\Lambda + \theta_1 S^0) \\
&= \frac{\theta_1(1-\epsilon_1-\epsilon_2)\Lambda(\theta_2+\mu)}{(\theta_1+\mu)(\epsilon_1\Lambda + \theta_1 S^0)}.
\end{aligned}$$

Then

$$\begin{aligned}
\mathcal{L}Y_1 \leq & \frac{\epsilon_1\Lambda}{V_{(i)}} + (c_1 + 1 - \eta_1)\bar{\beta} \\
& \exp(b(t))I + \theta_2 + \mu - \frac{\theta_1 S^0(\theta_2+\mu)}{\epsilon_1\Lambda + \theta_1 S^0}, \\
= & -\frac{\epsilon_1\Lambda}{V_{(i)}} + (1 + c_1 - \eta_1)\bar{\beta}\exp(b(t))I + \frac{\epsilon_1\Lambda}{V_{(i)}^0}.
\end{aligned}$$

Further, we define

$$Y_2 = -\log V_{(ii)} + c_3 Y_1 + c_4 V_{(ii)},$$

where c_3 and c_4 will be defined in a subsequent stage of the proof. Let us now apply the Itô's formula

$$\begin{aligned}
\mathcal{L}Y_2 \leq & -\frac{\epsilon_2\Lambda}{V_{(ii)}} - \frac{\theta_2 V_{(i)}}{V_{(ii)}} \\
& + (1-\eta_2)\bar{\beta}\exp(b(t))I + \rho + \mu \\
& - \frac{c_3\epsilon_1\Lambda}{V_{(i)}} + c_3(1 + c_1 - \eta_1)\bar{\beta}\exp(b(t))I \\
& + \frac{c_3\epsilon_1\Lambda}{V_{(i)}^0} \\
& + c_4\epsilon_2\Lambda + c_4\theta_2 V_{(i)} \\
& - c_4(1-\eta_2)\bar{\beta}\exp(b(t))V_{(ii)}I - c_4(\rho+\mu)V_{(ii)} \\
\leq & -\frac{\epsilon_2\Lambda}{V_{(ii)}} - \frac{\theta_2 V_{(i)}}{V_{(ii)}} \\
& - c_4(\rho+\mu)V_{(ii)} + \rho + \mu + \frac{c_3\epsilon_1\Lambda}{V_{(ii)}} \\
& + c_4(\epsilon_2\Lambda + \theta_2 V_{(i)}^0) \\
& + \bar{\beta}\exp(b(t))I((1-\eta_2) + c_3(1 + c_1 - \eta_1)), \\
\leq & -\frac{\epsilon_2\Lambda}{V_{(ii)}} \\
& - 3\left\{c_3 c_4 \theta_2 (\rho+\mu)\epsilon_1\Lambda\right\}^{\frac{1}{3}} + \rho + \mu \\
& + \frac{c_3\epsilon_1\Lambda}{V_{(i)}^0} + c_4(\epsilon_2\Lambda \\
& + \theta_2 V_{(i)}^0) + ((1-\eta_2) + c_3(1 + c_1 - \eta_1)) \\
& \times \bar{\beta}\exp(b(t))I.
\end{aligned}$$

Subsequently, c_3 and c_4 can be chosen from the following equation:

$$\frac{c_3\epsilon_1\Lambda}{V_{(i)}^0} = c_4(\epsilon_2\Lambda + \theta_2 V_{(i)}^0) = \frac{\theta_2(\rho+\mu)V_{(i)}^0}{\epsilon_2\Lambda + \theta_2 V_{(i)}^0}.$$

Then

$$\begin{aligned}\mathcal{L}Y_2 \leq & -\frac{\epsilon_2\Lambda}{V_{(ii)}} - \frac{\theta_2(\rho+\mu)V^0_{(i)}}{\epsilon_2\Lambda+\theta_2 V^0_{(i)}} + \rho + \mu \\ & + ((1-\eta_2) + c_3(1+c_1-\eta_1))\bar{\beta}\exp(b(t))I, \\ = & -\frac{\epsilon_2\Lambda}{V_{(ii)}} + (\rho+\mu)\left(1 - \frac{\theta_2 V^0_{(i)}}{\epsilon_2\Lambda+\theta_2 V^0_{(i)}}\right) \\ & + +((1-\eta_2) + c_3(1+c_1-\eta_1))\bar{\beta}\exp(b(t))I, \\ = & -\frac{\epsilon_2\Lambda}{V_{(ii)}} + (\rho+\mu)\left(\frac{\epsilon_2\Lambda}{\epsilon_2\Lambda+\theta_2 V^0_{(i)}}\right) \\ & + ((1-\eta_2) + c_3(1+c_1-\eta_1))\bar{\beta}\exp(b(t))I, \\ = & -\frac{\epsilon_2\Lambda}{V_{(ii)}} + \frac{\epsilon_2\Lambda}{V^0_{(ii)}} + ((1-\eta_2) \\ & + c_3(1+c_1-\eta_1))\bar{\beta}\exp(b(t))I.\end{aligned}$$

Now, we can define another function Y_3 as

$$\begin{aligned}Y_3 = & -\log E + d_1 Y_1 + d_2 Y_2 \\ & -d_3 \log S - (d_4+d_5+d_6)\log I,\end{aligned}$$

where $d_1,\ d_2,\ d_3,\ d_4, d_5$ and d_6 will be defined in a subsequent step of the proof. Now, let us apply the Itô's formula again

$$\begin{aligned}\mathcal{L}Y_3 \leq & -\frac{\bar{\beta}\exp(b(t)SI)}{E} - \frac{(1-\eta_1)\bar{\beta}\exp(b(t))V_{(i)}I}{E} \\ & - \frac{(1-\eta_2)\bar{\beta}\exp(b(t))V_{(ii)}I}{E} + \phi + \tau + \mu \\ & - \frac{d_1\epsilon_1\Lambda}{V_{(i)}} + d_1(1+c_1-\eta_1)\bar{\beta}\exp(b(t))I \\ & + \frac{d_1\epsilon_1\Lambda}{V^0_{(i)}} - \frac{d_2\epsilon_2\Lambda}{V_{(ii)}} \\ & + \frac{d_2\epsilon_2\Lambda}{V^0_{(ii)}} - d_7 \\ & + d_2((1-\eta_2) + c_3(1+c_1-\eta_1))\bar{\beta}\exp(b(t))I \\ & - \frac{d_3(1-\epsilon_1-\epsilon_2)\Lambda}{S} \\ & + d_3\bar{\beta}\exp(b(t))\,I + d_3(\theta_1+\mu) \\ & - \frac{(d_4+d_5+d_6)\phi E}{I} + (d_4+d_5+d_6) \\ & \times(\lambda+\omega+\mu) + d_7,\end{aligned}$$

where d_7 will also be determined later. Now

$$\begin{aligned}\mathcal{L}Y_3 \leq & -4\left\{d_3d_4d_7\bar{\beta}\exp(b(t))(1-\epsilon_1-\epsilon_2)\Lambda\phi\right\}^{\frac{1}{4}} \\ & - 3\left\{d_1d_5(1-\eta_1)\epsilon_1\Lambda\bar{\beta}\exp(b(t))\phi\right\}^{\frac{1}{3}} \\ & - 3\left\{d_2d_6(1-\eta_2)\epsilon_2\Lambda\phi\bar{\beta}\exp(b(t))\right\}^{\frac{1}{3}} \\ & + \phi + \tau + \mu + \frac{d_1\epsilon_1\Lambda}{V^0_{(i)}} + \frac{d_2\epsilon_2\Lambda}{V^0_{(ii)}} \\ & + d_3(\theta_1+\mu) \\ & + \bar{\beta}\exp(b(t))I\,(d_1(1+c_1-\eta_1) \\ & + d_2((1-\eta_2) + c_3(1+c_1-\eta_1)) + d_3) \\ & + (d_4+d_5+d_6)(\lambda+\omega+\mu), \\ = & -4\left\{d_3d_4d_7\bar{\beta}\exp\left(\frac{\kappa_2^2}{16\kappa_1}\right)(1-\epsilon_1-\epsilon_2)\Lambda\phi\right\}^{\frac{1}{4}} \\ & - 3\left\{d_1d_5(1-\eta_1)\epsilon_1\Lambda\bar{\beta}\exp\left(\frac{\kappa_2^2}{12\kappa_1}\right)\phi\right\}^{\frac{1}{3}} \\ & - 3\left\{d_2d_6(1-\eta_2)\epsilon_2\Lambda\phi\bar{\beta}\exp\left(\frac{\kappa_2^2}{12\kappa_1}\right)\right\}^{\frac{1}{3}} \\ & + \phi + \tau + \mu + \frac{d_1\epsilon_1\Lambda}{V^0_{(i)}} + \frac{d_2\epsilon_2\Lambda}{V^0_{(ii)}} \\ & + d_3(\theta_1+\mu) \\ & + (d_4+d_5+d_6)(\lambda+\omega+\mu) + d_7 \\ & + d_8\exp(b(t))I + h_1(b),\end{aligned}$$

where

$$d_8 = ((1+c_1-\eta_1)(d_1+c_3d_2) + d_2(1-\eta_2) + d_3)\,\bar{\beta},$$

and

$$\begin{aligned}h_1(b(t)) = & 4\left\{d_3d_4d_7\bar{\beta}(1-\epsilon_1-\epsilon_2)\Lambda\phi\right\}^{\frac{1}{4}} \\ & \left(\exp\left(\frac{\kappa_2^2}{64\kappa_1}\right) - \exp\left(\frac{b(t)}{4}\right)\right) \\ & + 3\left\{d_1d_5(1-\eta_1)\epsilon_1\Lambda\bar{\beta}\phi\right\}^{\frac{1}{3}} \\ & \left(\exp\left(\frac{\kappa_2^2}{36\kappa_1}\right) - \exp\left(\frac{b(t)}{3}\right)\right) \\ & + 3\left\{d_2d_6(1-\eta_2)\epsilon_2\Lambda\phi\bar{\beta}\right\}^{\frac{1}{3}} \\ & \times\left(\exp\left(\frac{\kappa_2^2}{36\kappa_1}\right) - \exp\left(\frac{b(t)}{3}\right)\right),\end{aligned}$$

where $d_1,\ d_2,\ d_3,\ d_4,\ d_5,\ d_6$ and d_7 are chosen in the following manner:

$$\frac{d_1}{V_{(i)}^0} = d_5(\lambda+\omega+\mu) = \frac{(1-\eta_1)\phi\bar{\beta}V_{(i)}^0 \exp\left(\frac{\kappa_2^2}{12\kappa_1}\right)}{\lambda+\omega+\mu},$$

$$+\phi+\tau+\mu+d_8\exp(b(t))\,I+h_1(b(t)) = -\left(R_0^s-1\right)(\phi+\tau+\mu) + d_8\exp(b(t))\,I+h_1(b(t)),$$

where

$$R_0^s = \frac{\bar{\beta}\phi\left\{S^0\exp\left(\frac{\kappa_2^2}{16\kappa_1}\right)+(1-\eta_2)V_{(i)}^0\exp\left(\frac{\kappa_2^2}{12\kappa_1}\right)+(1-\eta_2)V_{(ii)}^0\exp\left(\frac{\kappa_2^2}{12\kappa_1}\right)\right\}}{(\lambda+\omega+\mu)(\phi+\tau+\mu)}.$$

$$\frac{d_2}{V_{(ii)}^0} = d_6(\lambda+\omega+\mu) = \frac{(1-\eta_2)\phi\bar{\beta}V_{(ii)}^0\exp\left(\frac{\kappa_2^2}{12\kappa_1}\right)}{\lambda+\omega+\mu},$$

$$d_3(\theta_1+\mu) = d_4(\lambda+\omega+\mu) = d_7 = \frac{(1-\epsilon_1-\epsilon_2)\Lambda\bar{\beta}\exp\left(\frac{\kappa_2^2}{16\kappa_1}\right)}{(\theta_1+\mu)(\lambda+\omega+\mu)}.$$

Now, we have

$$\begin{aligned}\mathcal{L}Y_3 \le & -\frac{(1-\epsilon_1-\epsilon_2)\Lambda\phi\bar{\beta}\exp\left(\frac{\kappa_2^2}{16\kappa_1}\right)}{\theta_1+\mu} - \frac{(1-\eta_1)\epsilon_1\Lambda\phi\bar{\beta}V_{(i)}^0\exp\left(\frac{\kappa_2^2}{12\kappa_1}\right)}{\lambda+\omega+\mu} - \frac{(1-\eta_2)\epsilon_2\Lambda\phi\bar{\beta}V_{(ii)}^0\exp\left(\frac{\kappa_2^2}{12\kappa_1}\right)}{\lambda+\omega+\mu} \\ & +\phi+\tau+\mu+d_8\exp(b(t))I+h_1(b(t)), \\ = & -\frac{S^0\phi\bar{\beta}\exp\left(\frac{\kappa_2^2}{16\kappa_1}\right)}{\lambda+\omega+\mu} - \frac{(1-\eta_1)\phi\bar{\beta}V_{(i)}^0\exp\left(\frac{\kappa_2^2}{12\kappa_1}\right)}{\lambda+\omega+\mu} - \frac{(1-\eta_2)\phi\bar{\beta}V_{(ii)}^0\exp\left(\frac{\kappa_2^2}{12\kappa_1}\right)}{\lambda+\omega+\mu}\end{aligned}$$

Now, by utilizing the Young's inequality, we can write

$$\exp(b(t)) \le a_1\exp(2b(t)) + \frac{1}{4a_1}.$$

Further

$$\begin{aligned}\mathcal{L}Y_3 \le & -\left(R_0^s-1\right)(\phi+\tau+\mu) + d_8\left(a_1\exp(2b(t))+\frac{1}{4a_1}\right)I+h_1(b(t)), \\ \le & -\left(R_0^s-1\right)(\phi+\tau+\mu) + \frac{d_8a_1\exp(2b(t))\Lambda}{\mu}+\frac{d_8I}{4a_1}+h_1(b(t)), \\ = & -\left(R_0^s-1\right)(\phi+\tau+\mu) + \frac{d_8a_1\exp\left(\frac{\kappa_2^2}{\kappa_1}\right)\Lambda}{\mu} + \frac{d_8I}{4a_1}+h_1(b(t))+h_2(b(t)),\end{aligned}$$

where

$$h_2(b(t)) = \frac{d_8a_1\Lambda}{\mu}\left(\exp(2b(t)) - \exp\left(\frac{\kappa_2^2}{\kappa_1}\right)\right).$$

Now, let us choose a_1 such that

$$\frac{d_8a_1\exp\left(\frac{\kappa_2^2}{\kappa_1}\right)\Lambda}{\mu} = \frac{\left(R_0^s-1\right)(\phi+\tau+\mu)}{2}.$$

Now, it can be written that

$$\mathcal{L}Y_3 \le -\frac{\left(R_0^s-1\right)(\phi+\tau+\mu)}{2} + \frac{d_8I}{4a_1}+h_1(b(t))+h_2(b(t)).$$

Further let us define

$$Y_4 = Y_3 + \frac{\frac{d_8I}{4a_1}}{\lambda+\omega+\mu}.$$

Utilizing Itô's formula on Y_4, one can obtain

$$\begin{aligned}\mathcal{L}Y_4 &\leq -\frac{\left(R_0^s-1\right)(\phi+\tau+\mu)}{2}+h_1(b(t))+h_2(b(t))\\ &\quad+\frac{d_8 I}{4a_1}+\frac{\frac{d_8}{4a_1}}{\lambda+\omega+\mu}(\phi E-(\lambda+\omega+\mu)I),\\ &=-\frac{\left(R_0^s-1\right)(\phi+\tau+\mu)}{2}+h_1(b(t))\\ &\quad+h_2(b(t))+\frac{d_8\phi E}{4a_1(\lambda+\omega+\mu)},\\ &=-\frac{\left(R_0^s-1\right)(\phi+\tau+\mu)}{2}\\ &\quad+h_1(b(t))+h_2(b(t))+a_2E,\end{aligned}$$

where

$$a_2=\frac{d_8\phi}{4a_1(\lambda+\omega+\mu)}.$$

Now let us define the following functions:

$$\begin{aligned}Y_5 &=-\log S-\log V_{(i)}-\log V_{(ii)}-\log I\\ &\quad-\log(S^0-S)-\log(V_{(i)}^0-V_{(i)})\\ &\quad-\log(V_{(ii)}^0-V_{(ii)})-\log\left(\frac{\Lambda}{\mu}-A\right)\end{aligned}$$

and

$$Y_6=\exp(b(t))-b(t)-1.$$

Again by utilizing the Itô's formula, we get

$$\begin{aligned}\mathcal{L}Y_5 &\leq -\frac{(1-\epsilon_1-\epsilon-2)\Lambda}{S}+\bar{\beta}\exp(b(t))I\\ &\quad+\theta_1+\mu-\frac{\epsilon_1\Lambda}{V_{(i)}}-\frac{\theta_1 S}{V_{(i)}}\\ &\quad+(1-\eta_1)\bar{\beta}\exp(b(t))I+\theta_2\\ &\quad+\mu-\frac{\epsilon_2\Lambda}{V_{(ii)}}-\frac{\theta_2 V_{(i)}}{V_{(ii)}}\\ &\quad+(1-\eta_2)\bar{\beta}\exp(b(t))I+\rho\\ &\quad+\mu-\frac{\phi E}{I}+\lambda+\omega+\mu\\ &\quad+\frac{1}{S^0-S}\left((1-\epsilon_1-\epsilon_2)\Lambda\right.\\ &\quad\left.-\bar{\beta}\exp(b(t))SI-(\theta_1+\mu)S\right)\\ &\quad+\frac{1}{V_{(i)}^0-V_{(i)}}\left(\epsilon_1\Lambda+\theta_1 S\right.\\ &\quad\left.-(1-\eta_1)\bar{\beta}\exp(b(t))V_{(i)}I-(\theta_2+\mu)V_{(i)}\right)\\ &\quad+\frac{1}{V_{(ii)}^0-V_{(ii)}}\left(\epsilon_2\Lambda+\theta_2 V_{(i)}\right.\\ &\quad\left.-(1-\eta_2)\bar{\beta}\exp(b(t))V_{(ii)}I-(\rho+\mu)V_{(ii)}\right)\\ &\quad+\frac{1}{\left(\frac{\Lambda}{\mu}-A\right)}(\Lambda-\mu A-\tau E-(\lambda+\omega)I),\\ &\leq -\frac{(1-\epsilon_1-\epsilon-2)\Lambda}{S}-\frac{\epsilon_1\Lambda}{V_{(i)}}\\ &\quad-\frac{\epsilon_2\Lambda}{V_{(ii)}}-\frac{\phi E}{I}\\ &\quad+(3-\eta_1-\eta_2)\bar{\beta}\exp(b(t))I+\theta_1+\theta_2+\rho+\lambda\\ &\quad+\omega+4\mu+\frac{\Lambda-\mu A-\tau E-(\lambda+\omega)I}{\frac{\Lambda}{\mu}-A}\\ &\quad+\frac{1}{S-S^0}\left((\theta_1+\mu)(S^0-S)-\bar{\beta}\exp(b(t))SI\right)\\ &\quad+\frac{1}{V_{(i)}^0-V_{(i)}}\left((\theta_2+\mu)(V_{(i)}^0-V_{(i)})\right.\\ &\quad\left.-(1-\eta_1)\bar{\beta}\exp(b(t))V_{(i)}I\right)\\ &\quad+\frac{1}{V_{(ii)}^0-V_{(ii)}}\left((\rho+\mu)(V_{(i)}^0-V_{(i)})\right.\\ &\quad\left.-(1-\eta_2)\bar{\beta}\exp(b(t))V_{(ii)}I\right),\\ &\leq -\frac{(1-\epsilon_1-\epsilon-2)\Lambda}{S}-\frac{\epsilon_1\Lambda}{V_{(i)}}\\ &\quad-\frac{\epsilon_2\Lambda}{V_{(ii)}}-\frac{\phi E}{I}-\frac{\bar{\beta}\exp(b(t))SI}{S^0-S}\\ &\quad-\frac{(1-\eta_1)\bar{\beta}\exp(b(t))V_{(i)}I}{V_{(i)}^0-V_{(i)}}\\ &\quad-\frac{(1-\eta_2)\bar{\beta}\exp(b(t))V_{(ii)}I}{V_{(ii)}^0-V_{(ii)}}\\ &\quad-\frac{\tau E}{\frac{\Lambda}{\mu}-A}+\frac{(3-\eta_1-\eta_2)\bar{\beta}\exp(b(t))}{\mu}\\ &\quad+2\theta_1+2\theta_2+2\rho+\lambda+\omega+8\mu.\end{aligned}$$

Also, we have

$$\mathcal{L}Y_6=-\kappa_1 b(t)(\exp(b(t))-1)+\frac{\kappa_2^2\exp(b(t))}{2}.$$

Now let us define

$$Y_7=PY_4+Y_5+Y_6,$$

where P is chosen to be sufficiently large and satisfy

$$-\frac{P(R_0^s-1)(\phi+\tau+\mu)}{2}+\mathcal{J}_1 +2\theta_1+2\theta_2+2\rho+\lambda+\omega+8\mu\le -2,$$

where

$$\mathcal{J}_1=\sup_{b(t)\in\mathbb{R}}\{-\kappa_1 b(t)(\exp(b(t))-1) +\left(\frac{\kappa_2^2}{2}+\frac{(3-\eta_1-\eta_2)\bar{\beta}\Lambda}{\mu}\right) \exp(b(t))\}.$$

Further, we have

$$\mathcal{L}Y_7\le Ph_1(b(t))+Ph_2(b(t))+h_3(S,V_{(i)},V_{(i)},E,I),$$

where

$$\begin{aligned}
&h_3(S,V_{(i)},V_{(ii)},E,I,b)\\
&=-\frac{P(R_0^s-1)(\phi+\tau+\mu)}{2}\\
&+Pa_2E-\frac{(1-\epsilon_1-\epsilon-2)\Lambda}{S}-\frac{\epsilon_1\Lambda}{V_{(i)}}\\
&-\frac{\epsilon_2\Lambda}{V_{(ii)}}-\frac{\phi E}{I}\\
&-\frac{\bar{\beta}\exp(b(t))SI}{S^0-S}-\frac{(1-\eta_1)\bar{\beta}\exp(b(t))V_{(i)}I}{V_{(i)}^0-V_{(i)}}\\
&-\frac{(1-\eta_2)\bar{\beta}\exp(b(t))V_{(ii)}I}{V_{(ii)}^0-V_{(ii)}}\\
&-\frac{\tau E}{\frac{\Lambda}{\mu}-S-V_{(i)}-V_{(ii)}-E-I}\\
&+\left(\frac{\kappa_2^2}{2}+\frac{(3-\eta_1-\eta_2)\bar{\beta}\Lambda}{\mu}\right)\exp(b(t))\\
&-\kappa_1 b(t)(\exp(b(t))-1)+2\theta_1\\
&+2\theta_2+2\rho+\lambda+\omega+8\mu
\end{aligned}$$

Step 2 (Construction of a compact set)
We define a compact set as follows:

$$\frac{\kappa_1}{2}(1-m)\log m+\sup_{b(t)\in\mathbb{R}}\{h_4(b(t))\} +2\theta_1+2\theta_2+2\rho+\lambda+\omega+8\mu+\frac{Pa_2\Lambda}{\mu}\le -1, \tag{5}$$

$$\frac{\kappa_1}{2}\left(\frac{1}{m}-1\right)\log m+\sup_{b(t)\in\mathbb{R}}\{h_4(b(t))\} +2\theta_1+2\theta_2+2\rho+\lambda+\omega+8\mu+\frac{Pa_2\Lambda}{\mu}\le -1, \tag{6}$$

$$\frac{Pa_2\Lambda}{\mu}\le 1, \tag{7}$$

$$\frac{Pa_2\Lambda}{\mu}-2-\frac{\min\{(1-\epsilon_1-\epsilon_2),\epsilon_1\Lambda,\epsilon_2\Lambda,\phi\}}{m}\le -1, \tag{8}$$

$$\frac{Pa_2\Lambda}{\mu}-\frac{1}{m}\min\{\bar{\beta},(1-\eta_1)\bar{\beta},(1-\eta_2)\bar{\beta},\tau\}-2\le -1. \tag{9}$$

Here

$$h_4(b(t))=\frac{-\kappa_1 b(t)(\exp(b(t))-1)}{2} +\left(\frac{\kappa_2^2}{2}+\frac{(3-\eta_1-\eta_2)\bar{\beta}\Lambda}{\mu}\right)\exp(b(t)).$$

To prove that $h_3(S,V_{(i)},V_{(ii)},E,I,b)<-1,\ \forall\ (S,V_{(i)},V_{(i)},E,I,b)\in\Theta\backslash\mathbb{D}$, let us define the following sub-domains:

$$\begin{aligned}
\mathbb{D}_1^C&=\{(S,V_{(i)},V_{(ii)},E,I,b)\in\theta:0<\exp(b(t))<m\},\\
\mathbb{D}_2^C&=\left\{(S,V_{(i)},V_{(ii)},E,I,b)\in\theta:\frac{1}{m}<\exp(b(t))\right\},\\
\mathbb{D}_3^C&=\{(S,V_{(i)},V_{(ii)},E,I,b)\in\theta:0<E<m\},\\
\mathbb{D}_4^C&=\{(S,V_{(i)},V_{(ii)},E,I,b)\in\theta:0<S<m\},\\
\mathbb{D}_5^C&=\{(S,V_{(i)},V_{(ii)},E,I,b)\in\theta:0<V_{(i)}<m\},\\
\mathbb{D}_6^C&=\{(S,V_{(i)},V_{(ii)},E,I,b)\in\theta:0<V_{(ii)}<m\},\\
\mathbb{D}_7^C&=\left\{(S,V_{(i)},V_{(ii)},E,I,b)\in\theta:m\le E,\ 0<I<m^2\right\},
\end{aligned}$$

$$\mathbb{D}_m=\left\{(S,V_{(i)},V_{(ii)},E,I,b)\in\Theta\ :\ \begin{array}{r}m\le\exp(b(t))\le\frac{1}{m},\ m\le S,\ m\le V_{(i)},\ m\le V_{(ii)},\ m\le E,\\ m^2\le I,\ S\le S^0-m^5,\ V_{(i)}\le V_{(i)}^0-m^5,\ V_{(ii)}\le V_{(ii)}^0-m^5,\\ S+V_{(i)}+V_{(ii)}+E+I\le\frac{\Lambda}{\mu}-m^2\end{array}\right\},$$

with $m\in(0,1)$ is a small enough constant satisfying the following inequalities:

$$\mathbb{D}_8^C=\{(S,V_{(i)},V_{(ii)},E,I,b)\in\theta:m\le S, \ m\le\exp(b(t)),\ m^2\le I,\ S^0-m^5<S\},$$

$$\mathbb{D}_9^C = \Big\{(S, V_{(i)}, V_{(ii)}, E, I, b) \in \theta : m \le S, \; m \le \exp(b(t)), \; m^2 \le I, \; V_{(i)}^0 - m^5 < V_{(i)}\Big\},$$
$$\mathbb{D}_{10}^C = \Big\{(S, V_{(i)}, V_{(ii)}, E, I, b) \in \theta : m \le S, \; m \le \exp(b(t)), \; m^2 \le I, \; V_{(ii)}^0 - m^5 < V_{(ii)}\Big\},$$
$$\mathbb{D}_{11}^C = \Big\{(S, V_{(i)}, V_{(ii)}, E, I, b) \in \theta : m \le E, \; \frac{\Lambda}{\mu} - m^2 < S + V_{(i)} + V_{(ii)} + E + I\Big\}.$$

Further, it can be easily verified that

$$\Theta \backslash \mathbb{D} = \mathbb{D}_1^C \cup \mathbb{D}_2^C \cup \mathbb{D}_3^C \cup \mathbb{D}_4^C \cup \mathbb{D}_5^C \cup \mathbb{D}_6^C \cup \mathbb{D}_7^C \cup \mathbb{D}_8^C \cup \mathbb{D}_9^C \cup \mathbb{D}_{10}^C \cup \mathbb{D}_{11}^C.$$

our aim is to prove that $h_3(S, V_{(i)}, V_{(ii)}, E, I, b) < -1$, in each of these sub-domains. For that, consider the following cases coupled with equations (5)-(9):

Case (i). For any $(S, V_{(i)}, V_{(ii)}, E, I, b) \in \mathbb{D}_1^C, \; b(t) \in (-\infty, \; \log(m))$. Now

$$\begin{aligned} &h_3(S, V_{(i)}, V_{(ii)}, E, I, b) \\ &\le -\kappa_1 b(t)(\exp(b(t)) - 1) \\ &+ \left(\frac{\kappa_2^2}{2} + \frac{(3 - \eta_1 - \eta_2)\bar{\beta}\Lambda}{\mu}\right)\exp(b(t)) \\ &+ 2\theta_1 + 2\theta_2 + 2\rho + \lambda + \omega + 8\mu + \frac{Pa_2\Lambda}{\mu}, \\ &\le \frac{-\kappa_1 b(t)(\exp(b(t)) - 1)}{2} + \sup_{b(t)\in\mathbb{R}}\{h_4(b(t))\} \\ &+ 2\theta_1 + 2\theta_2 + 2\rho + \lambda + \omega + 8\mu + \frac{Pa_2\Lambda}{\mu}. \end{aligned}$$

Then

$$\begin{aligned} &h_3(S, V_{(i)}, V_{(ii)}, E, I, b) \\ &\le \frac{\kappa_1}{2}(1 - m)\log m \\ &+ \sup_{b(t)\in\mathbb{R}}\{h_4(b(t))\} + 2\theta_1 + 2\theta_2 + 2\rho \\ &+ \lambda + \omega + 8\mu + \frac{Pa_2\Lambda}{\mu}, \\ &\le -1. \end{aligned}$$

Case (ii). For any $(S, V_{(i)}, V_{(ii)}, E, I, b) \in \mathbb{D}_2^C, \; b(t) \in (-\log(m), \; \infty)$. Now

$$\begin{aligned} &h_3(S, V_{(i)}, V_{(ii)}, E, I, b) \\ &\le -\kappa_1 b(t)(\exp(b(t)) - 1) + \sup_{b(t)\in\mathbb{R}}\{h_4(b(t))\} \\ &+ 2\theta_1 + 2\theta_2 + 2\rho + \lambda + \omega + 8\mu + \frac{Pa_2\Lambda}{\mu}, \\ &\le \frac{\kappa_1}{2}\left(\frac{1}{m} - 1\right)\log m + \sup_{b(t)\in\mathbb{R}}\{h_4(b(t))\} \\ &+ 2\theta_1 + 2\theta_2 + 2\rho + \lambda + \omega + 8\mu + \frac{Pa_2\Lambda}{\mu}, \\ &\le -1. \end{aligned}$$

Case (iii). For any $(S, V_{(i)}, V_{(ii)}, E, I, b) \in \mathbb{D}_3^C$. Now

$$\begin{aligned} h_3(S, V_{(i)}, V_{(ii)}, E, I, b) &\le \frac{Pa_2\Lambda}{\mu} - 2, \\ &\le -1. \end{aligned}$$

Case (iv). For any $(S, V_{(i)}, V_{(ii)}, E, I, b) \in \mathbb{D}_4^C$ or $\mathbb{D}_5^C$ or $\mathbb{D}_6^C$ or $\mathbb{D}_7^C$. Now

$$\begin{aligned} &h_3(S, V_{(i)}, V_{(ii)}, E, I, b) \\ &\le \frac{Pa_2\Lambda}{\mu} - 2 - \frac{(1 - \epsilon_1 - \epsilon - 2)\Lambda}{S} \\ &- \frac{\epsilon_1\Lambda}{V_{(i)}} - \frac{\epsilon_2\Lambda}{V_{(ii)}} - \frac{\phi E}{I}, \\ &\le \frac{Pa_2\Lambda}{\mu} - 2 \\ &- \frac{\min\{(1 - \epsilon_1 - \epsilon_2), \epsilon_1\Lambda, \epsilon_2\Lambda, \phi\}}{m}, \\ &\le -1. \end{aligned}$$

Case (v). For any $(S, V_{(i)}, V_{(ii)}, E, I, b) \in \mathbb{D}_8^C$ or $\mathbb{D}_9^C$ or $\mathbb{D}_{10}^C$ or $\mathbb{D}_{11}^C$. Now

$$\begin{aligned} &h_3(S, V_{(i)}, V_{(ii)}, E, I, b) \\ &\le \frac{Pa_2\Lambda}{\mu} - \frac{\bar{\beta}\exp(b(t))SI}{S^0 - S} \\ &- \frac{(1 - \eta_1)\bar{\beta}\exp(b(t))V_{(i)}I}{V_{(i)}^0 - V_{(i)}} \\ &- \frac{(1 - \eta_2)\bar{\beta}\exp(b(t))V_{(ii)}I}{V_{(ii)}^0 - V_{(ii)}} \\ &- \frac{\tau E}{\frac{\Lambda}{\mu} - S - V_{(i)} - V_{(ii)} - E - I} - 2, \\ &\le \frac{Pa_2\Lambda}{\mu} - \frac{1}{m} \\ &\min\{\bar{\beta}, (1 - \eta_1)\bar{\beta}, (1 - \eta_2)\bar{\beta}, \tau\} - 2, \\ &\le -1. \end{aligned}$$

Now, from the cases (i)-(v), it can be stated that

$$h_3(S, V_{(i)}, V_{(ii)}, E, I, b) \leq -1, \ \forall\ (S, V_{(i)}, V_{(ii)}, E, I, b) \in \Theta \backslash \mathbb{D}.$$

Step 3 (**Existence of stationary distribution**) : Since the function Y_7 tends to ∞ as $S, V_{(i)}, V_{(ii)}, E, I, b$ and $S + V_{(i)} + V_{(ii)} + E + I$ approaches the boundary of Θ. Thus there exists a point $(\bar{S}, \bar{V_{(i)}}, \bar{V_{(ii)}}, \bar{E}, \bar{I})$ in the interior of θ which makes $Y_7(\bar{S}, \bar{V_{(i)}}, \bar{V_{(ii)}}, \bar{E}, \bar{I})$ takes the minimum value. Now, take U_2 as $U_2 = Y_7(S, V_{(i)}, V_{(ii)}, E, I, b) - Y_7(\bar{S}, \bar{V_{(i)}}, \bar{V_{(ii)}}, \bar{E}, \bar{I}, \bar{\beta})$, which is a non-negative C^2-function. Now, by applying Itô's formula

$$\mathcal{L}U_2 \leq h_3(S, V_{(i)}, V_{(ii)}, E, I, b) + Ph_2(b(t)) + Ph_1(b(t)).$$

Now, for any initial value $(S(0), V_{(i)}(0), V_{(ii)}(0), E(0), I(0), b(0)) \in \Theta$ and an interval $[0, t]$, applying mathematical induction will give

$$\begin{aligned}
0 &\leq \frac{\mathbb{E}\,(U_2(0))}{t} + \frac{1}{t}\int_0^t \mathbb{E}\,(\mathcal{L}U_2)\,ds, \\
&\leq \frac{\mathbb{E}\,(U_2(0))}{t} + \frac{1}{t}\int_0^t \mathbb{E}\left(h_3(S, V_{(i)}, V_{(ii)}, E, I, b)\right) ds \\
&+ 4P\left\{d_3d_4d_7\bar{\beta}(1-\epsilon_1-\epsilon_2)\Lambda\phi\right\}^{\frac{1}{4}} \\
&\left(\exp\left(\frac{\kappa_2^2}{64\kappa_1}\right) - \mathbb{E}\left(\frac{1}{t}\int_0^t \exp\left(\frac{b(s)}{4}\right) ds\right)\right) \\
&+ 3P\left((d_1d_5\epsilon_1\Lambda\bar{\beta}\phi(1-\eta_1))^{\frac{1}{3}}\right. \\
&\left.+(d_2d_6\epsilon_2\Lambda\bar{\beta}\phi(1-\eta_2))^{\frac{1}{3}}\right) \\
&\left(\exp\left(\frac{\kappa_2^2}{36\kappa_1}\right) - \mathbb{E}\left(\frac{1}{t}\int_0^t \exp\left(\frac{b(s)}{3}\right) ds\right)\right) \\
&+ \frac{Pd_8a_1\Lambda}{\mu}\left(\mathbb{E}\left(0\frac{1}{t}\int_0^t \exp\left(2b(s)\right) ds\right)\right. \\
&\left.- \exp\left(\frac{\kappa_2^2}{\kappa_1}\right)\right). \qquad (10)
\end{aligned}$$

By utilizing the Lemma 2, we have

$$\begin{aligned}
\lim_{t\to\infty}\frac{1}{t}\int_0^t \exp\left(\frac{b(s)}{4}\right) ds &= \exp\left(\frac{\kappa_2^2}{64\kappa_1}\right), \\
\lim_{t\to\infty}\frac{1}{t}\int_0^t \exp\left(\frac{b(s)}{3}\right) ds &= \exp\left(\frac{\kappa_2^2}{36\kappa_1}\right), \\
\lim_{t\to\infty}\frac{1}{t}\int_0^t \exp\left(2b(s)\right) ds &= \exp\left(\frac{\kappa_2^2}{\kappa_1}\right).
\end{aligned}$$

Now, by allowing $t \to \infty$ in (10), we get

$$\begin{aligned}
0 &\leq \liminf_{t\to\infty}\frac{\mathbb{E}\,(U_2(0))}{t} \\
&+ \liminf_{t\to\infty}\frac{1}{t}\int_0^t \mathbb{E}\left(h_3(S, V_{(i)}, V_{(ii)}, E, I, b)\right) ds, \\
&= \liminf_{t\to\infty}\frac{1}{t}\int_0^t \mathbb{E}\left(h_3(S, V_{(i)}, V_{(ii)}, E, I, b)\right) ds, \ \text{a.s.}
\end{aligned}$$

Also, we can write

$$h_3(S, V_{(i)}, V_{(ii)}, E, I, b) \leq Q, \quad \forall (S, V_{(i)}, V_{(ii)}, E, I, b) \in \theta$$

where

$$Q = \sup_{(S, V_{(i)}, V_{(ii)}, E, I, b)\in\Theta}\left\{\begin{array}{l} Pa_2E - \dfrac{(1-\epsilon_1-\epsilon-2)\Lambda}{S} - \dfrac{\epsilon_1\Lambda}{V_{(i)}} - \dfrac{\epsilon_2\Lambda}{V_{(ii)}} - \dfrac{\phi E}{I} \\ -\dfrac{\bar{\beta}\exp(b(t))SI}{S^0 - S} - \dfrac{(1-\eta_1)\bar{\beta}\exp(b(t))V_{(i)}I}{V_{(i)}^0 - V_{(i)}} \\ -\dfrac{(1-\eta_2)\bar{\beta}\exp(b(t))V_{(ii)}I}{V_{(ii)}^0 - V_{(ii)}} - \dfrac{\tau E}{\frac{\Lambda}{\mu} - S - V_{(i)} - V_{(ii)} - E - I} \end{array}\right\} < \infty.$$

Then, we have

$$\begin{aligned}
&\liminf_{t\to\infty}\frac{1}{t}\int_0^t \mathbb{E}\left(h_3(S,V_{(i)},V_{(ii)},E,I,b)\right)ds,\\
&\quad=\liminf_{t\to\infty}\frac{1}{t}\int_0^t \mathbb{E}\left(h_3(S,V_{(i)},V_{(ii)},E,I,b)\right)\\
&\mathbb{I}_{\{(S,V_{(i)},V_{(ii)},E,I,b)\in\mathbb{D}\}}ds\\
&\quad+\liminf_{t\to\infty}\frac{1}{t}\int_0^t \mathbb{E}\left(h_3(S,V_{(i)},V_{(ii)},E,I,b)\right)\\
&\mathbb{I}_{\{(S,V_{(i)},V_{(ii)},E,I,b)\in\Theta\setminus\mathbb{D}\}}ds,\\
&\quad\le Q\liminf_{t\to\infty}\frac{1}{t}\int_0^t \mathbb{I}_{\{(S,V_{(i)},V_{(ii)},E,I,b)\in\mathbb{D}\}}ds\\
&\quad-\liminf_{t\to\infty}\frac{1}{t}\int_0^t \mathbb{I}_{\{(S,V_{(i)},V_{(ii)},E,I,b)\in\Theta\setminus\mathbb{D}\}}ds,\\
&\quad\le (Q+1)\liminf_{t\to\infty}\frac{1}{t}\\
&\quad times\int_0^t \mathbb{I}_{\{(S,V_{(i)},V_{(ii)},E,I,b)\in\mathbb{D}\}}ds-1.
\end{aligned}$$

Further, it can be shown that

$$\begin{aligned}
\liminf_{t\to\infty}\frac{1}{t}\int_0^t \mathbb{I}_{\{(S,V_{(i)},V_{(ii)},E,I,b)\in\mathbb{D}\}}ds &\ge \frac{1}{Q+1}\\
&> 0,\ \text{a.s.}
\end{aligned}$$

Now, let $\mathbb{P}\left\{t,(S,V_{(i)},V_{(ii)},E,I,b),\Theta\right\}$ is the transition probability of $(S,V_{(i)},V_{(ii)},E,I,b)$ belongs to the set Θ. Further, on the utilization of the Fatou's lemma, we can write

$$\begin{aligned}
&\liminf_{t\to\infty}\frac{1}{t}\int_0^t \mathbb{P}\left\{s,(S,V_{(i)},V_{(ii)},E,I,b),\mathbb{D}\right\}ds\\
&\ge\frac{1}{Q+1}>0,\ \text{a.s.}
\end{aligned}$$

This establishes the existence of a stationary distribution on Θ. It can also be stated that this stationary distribution carries the Feller property also. This concludes the proof. □

4.3 Extinction of the infection from the stochastic model (3)

In this subsection, we derive the conditions that must be satisfied for the SARS-CoV-2 infection to be eradicated from the population. To achieve this, we introduce the stochastic threshold parameter for extinction R_0^e, defined as:

$$R_0^e=\sqrt{R_0^d}+\frac{\bar\beta\phi(S^0+(1-\eta_1)V_{(i)}^0+(1-\eta_2)V_{(ii)}^0)}{\sqrt{R_0^d}(\phi+\tau+\mu)\min\{\phi+\tau+\mu,\lambda+\omega+\mu\}}$$

$$\left(1+\exp\left(\frac{\kappa_2^2}{\kappa_1}\right)-2\exp\left(\frac{\kappa_2^2}{4\kappa_1}\right)\right)$$

This expression represents the threshold that combines both deterministic and stochastic effects, quantifying the conditions under which the infection will fade out over time. Satisfying these conditions is crucial for determining when public health interventions will successfully eliminate the virus from the population. For this, we establish the following theorem:

Theorem 4.4 *If $R_0^e<1$, the extinction of the exposed and infected individuals occur exponentially. Mathematically,*

$$\limsup_{t\to\infty}\frac{1}{t}\log\left\{\frac{\phi}{\sqrt{R_0^d}(\phi+\tau+\mu)(\lambda+\omega+\mu)}E(t)+\frac{1}{\lambda+\omega+\mu}I(t)\right\}<0\ a.s..$$

Proof Theorem 1.4 from [64] establishes the existence of a left positive eigenvector for the following two-dimensional matrix:

$$A=\begin{pmatrix}0 & \frac{\bar\beta(S^0+(1-\eta_1)V_{(i)}^0+(1-\eta_2)V_{(ii)}^0)}{\phi+\tau+\mu}\\ \frac{\phi}{\lambda+\omega+\mu} & 0\end{pmatrix}.$$

This eigenvector corresponds to $\sqrt{R_0^d}$ and satisfies the equation:

$$\sqrt{R_0^d}(\varpi,1)=(\varpi,1)A.$$

Now, define a C^2-function U_3 as folllows:

$$U_3=\left(\frac{\varpi}{\phi+\tau+\mu}\right)E+\left(\frac{1}{\lambda+\omega+\mu}\right)I.$$

Now, by applying the Itô's formula, we get

$$\begin{aligned}
\mathcal{L}(\log U_3)&=\frac{1}{U_3}\left\{\frac{\varpi}{\phi+\tau+\mu}\left(\bar\beta\exp(b(t))SI\right.\right.\\
&\quad+(1-\eta_1)\bar\beta\exp(b(t))V_{(i)}I\\
&\quad\left.+(1-\eta_2)\bar\beta\exp(b(t))V_{(ii)}I\right)\Big\}\\
&\quad+\frac{1}{U_3}\left\{\frac{1}{\lambda+\omega+\mu}\left(\phi E-(\lambda+\omega+\mu)I\right)\right\},\\
&\le\frac{1}{U_3}\left\{\frac{\varpi\bar\beta I\exp(b(t))}{\phi+\tau+\mu}\right.\\
&\quad\left(S^0+(1-\eta_1)V_{(i)}^0+(1-\eta_2)V_{(ii)}^0\right)\\
&\quad\left.-\frac{\varpi E}{\phi+\tau+\mu}+\frac{\phi E}{\lambda+\omega+\mu}-I\right\},
\end{aligned}$$

$$
\begin{aligned}
&= \frac{1}{U_3}\left\{\frac{\varpi\bar{\beta}I}{\phi+\tau+\mu}\right.\\
&\left(S^0+(1-\eta_1)V^0_{(i)}+(1-\eta_2)V^0_{(ii)}\right)\\
&-\frac{\varpi E}{\phi+\tau+\mu}\\
&\left.+\frac{\phi E}{\lambda+\tau+\mu}-I\right\}\\
&+\frac{I}{U_3}\left\{\frac{\varpi\bar{\beta}}{\phi+\tau+\mu}\right.\\
&\left(S^0+(1-\eta_1)V^0_{(i)}+(1-\eta_2)V^0_{(ii)}\right)\\
&|\exp(b(t))-1|\},\\
&\leq \frac{\varpi\bar{\beta}(\lambda+\omega+\mu)}{\phi+\tau+\mu}\\
&\left\{S^0+(1-\eta_1)V^0_{(i)}+(1-\eta_2)V^0_{(ii)}\right\}\\
&|\exp(b(t))-1|\\
&+\frac{1}{U_3}(\varpi,1)\left\{A(E,I)^T-(E,I)^T\right\},\\
&\leq \frac{\varpi\bar{\beta}(\lambda+\omega+\mu)}{\phi+\tau+\mu}\\
&\left\{S^0+(1-\eta_1)V^0_{(i)}+(1-\eta_2)V^0_{(ii)}\right\}\\
&|\exp(b(t))-1|\\
&+\frac{1}{U_3}R^d_0(\varpi,1)(E,I)^T-(\varpi,1)(E,I)^T\},\\
&= \frac{\varpi\bar{\beta}(\lambda+\omega+\mu)}{\phi+\tau+\mu}\\
&\left\{S^0+(1-\eta_1)V^0_{(i)}+(1-\eta_2)V^0_{(ii)}\right\}\\
&|\exp(b(t))-1|\\
&+\frac{1}{U_3}\left\{(\sqrt{R^d_0}-1)(\varpi E+I)\right\},\\
&= \frac{\bar{\beta}\phi}{\sqrt{R^d_0}\phi+\tau+\mu}\\
&\left\{S^0+(1-\eta_1)V^0_{(i)}+(1-\eta_2)V^0_{(ii)}\right\}\\
&|\exp(b(t))-1|\\
&-\min\{\phi+\tau+\mu,\lambda+\omega+\mu\}\\
&\times\left(1-\sqrt{R^d_0}\right). \qquad (11)
\end{aligned}
$$

Now, we integrate (11) from 0 to t on both the sides and get

$$
\begin{aligned}
&\frac{\log U_3-\log U_3(0)}{t}\\
&\leq \frac{\bar{\beta}\phi}{\sqrt{R^d_0}\phi+\tau+\mu}\\
&\left\{S^0+(1-\eta_1)V^0_{(i)}+(1-\eta_2)V^0_{(ii)}\right\}\\
&\left(\frac{1}{t}\int_0^t|\exp(b(s))-1|ds\right)\\
&-\min\{\phi+\tau+\mu,\lambda+\omega+\mu\}\left(1-\sqrt{R^d_0}\right). \qquad (12)
\end{aligned}
$$

Subsequently, on both the sides of (12), we take the limit supremum and use Lemma 2

$$
\begin{aligned}
&\limsup_{t\to\infty}\frac{\log U_3(t)}{t}\\
&\leq \frac{\bar{\beta}\phi}{\sqrt{R^d_0}\phi+\tau+\mu}\\
&\left\{S^0+(1-\eta_1)V^0_{(i)}+(1-\eta_2)V^0_{(ii)}\right\}\\
&\left\{1+\exp\left(\frac{\kappa_2^2}{\kappa_1}\right)-2\exp\left(\frac{\kappa_2^2}{4\kappa_1}\right)\right\}^{\frac{1}{2}}\\
&-\min\{\phi+\tau+\mu,\lambda+\omega+\mu\}\left(1-\sqrt{R^d_0}\right),\\
&=-\min\{\phi+\tau+\mu,\lambda+\omega+\mu\}\left(1-\sqrt{R^e_0}\right),
\end{aligned}
$$

where

$$
\begin{aligned}
R^e_0 = \sqrt{R^d_0}+&\frac{\bar{\beta}\phi(S^0+(1-\eta_1)V_{(i)}+(1-\eta_2)V_{(ii)})}{\sqrt{R^d_0}(\phi+\tau+\mu)\min\{\phi+\tau+\mu,\lambda+\omega+\mu\}}\\
&\left(1+\exp\left(\frac{\kappa_2^2}{\kappa_1}\right)-2\exp\left(\frac{\kappa_2^2}{4\kappa_1}\right)\right).
\end{aligned}
$$

That is the infection will extinct exponentially with probability one, when $R^e_0 < 1$. This concludes the proof. □

5 Numerical simulations and discussion

In this section, numerical simulations of the stochastic model are presented, highlighting their crucial role

in disease control and prevention. These simulations provide an understanding of the complex dynamics of SARS-CoV-2 transmission and progression, allowing researchers to explore various scenarios and interventions without the limitations of real-world constraints. By simulating the stochastic behavior of the epidemic, we gain insights into prevention strategies, treatment effectiveness and future trends. This information aids public health officials and policymakers in designing effective measures, optimizing resources and reducing the impact of the disease, thereby supporting evidence-based decision-making for future outbreaks. For the model (3), we write the following discretized scheme by applying Milstein's higher-order method [65] which is widely used for the numerical simulations of SDEs:

$$
\begin{aligned}
b^{(k+1)} &= b^{(k)} - \kappa_1 b^{(k)}\Delta t + \kappa_1 x^{(k)}\sqrt{\Delta t},\\
S^{(k+1)} &= S^{(k)} + [(1-\epsilon_1-\epsilon_2)\Lambda\\
&\quad -\bar{\beta}\exp\left(b^{(k)}\right) S^{(k)} I^{(k)} - (\theta_1+\mu)S^{(k)}\Big]\Delta t,\\
V_{(i)}^{(k+1)} &= V_{(i)}^{(k)} + \Big[\epsilon_1\Lambda + \theta_1 S^{(k)} - (1-\eta_1)\bar{\beta}\\
&\quad \exp\left(b^{(k)}\right) V_{(i)}^{(k)} I^{(k)} - (\theta_2+\mu)V_{(i)}^{(k)}\Big]\Delta t,\\
V_{(ii)}^{(k+1)} &= V_{(ii)}^{(k)} + \Big[\epsilon_2\Lambda + \theta_2 V_{(ii)}^{(k)} - (1-\eta_2)\bar{\beta}\\
&\quad \exp\left(b^{(k)}\right) V_{(ii)}^{(k)} I^{(k)} - (\rho+\mu)V_{(ii)}^{(k)}\Big]\Delta t,\\
E^{(k+1)} &= E^{(k)} + \Big[\bar{\beta}\exp\left(b^{(k)}\right) I^{(k)}\\
&\quad \left(S^{(k)} + (1-\eta_1)V_{(i)}^{(k)} + (1-\eta_2)V_{(ii)}^{(k)}\right)\\
&\quad -(\phi+\tau+\mu)E^{(k)}\Big]\Delta t,\\
I^{(k+1)} &= I^{(k)} + \Big[\phi E^{(k)} - (\lambda+\omega+\mu)I^{(k)}\Big]\Delta t.
\end{aligned}
$$

Here $(S^{(k)}, V_{(i)}^{(k)}, V_{(ii)}^{(k)}, E^{(k)}, I^{(k)}, b^{(k)})$ represents the values at the k-th iteration of the discretization equation. Also, independent random variables following a standard normal distribution are represented as $x^{(k)}$. Further, the time increment is denoted as Δt which is always positive.

5.1 Model calibration and parameter estimation through data fitting

We gathered weekly data of COVID-19 confirmed cases in India from the official website of the World Health Organization [66], covering the period from February 28, 2021 to May 02, 2021. This time-frame corresponds to the second wave of the epidemic in India, specifically when the number of cases was increasing and reaching the peak of infection. We applied a non-linear least squares fitting routine using the *lsqcurvefit* function in MATLAB R2023b to fit the model (3) to the data. By focusing on this critical period of rising cases, we aimed to understand the impact of the control measures and preventive actions implemented by public health agencies. This approach allows us to evaluate how these interventions influenced the duration and severity of the second wave under various conditions.

Firstly, the average life expectancy of an individual in India in 2021 was 67.24 years [67]. Using this, the natural mortality rate can be calculated as $\dfrac{1}{67.24\times 52} = 0.000286$ weeks^{-1}. Additionally, the total population of India in 2021 was estimated to be 1,400 million [67]. This allows us to determine the recruitment rate as $\Lambda = N\mu = 0.4$ million. All other parameters, along with their descriptions, values and sources, are provided in Table 2. Also, the estimated initial conditions are presented in Table 3. The fitting of the model with the real data is plotted in Fig. 2.

Further, the residual errors are computed to evaluate how well the model fits the actual data, with each residual error defined as:

$$\text{Residual}_i = I_{\text{data}}(t_i) - I_{\text{model}}(t_i),$$

where $I_{\text{data}}(t_i)$ represents the observed number of COVID-19 cases at time t_i and $I_{\text{model}}(t_i)$ denotes the predicted number of the model at the same time point. The residuals, illustrated in Fig. 3a, show a high degree of fit. To further assess the accuracy of the model, we calculated two error metrics: Mean Absolute Percentage Error (MAPE) and Root Mean Squared Error (RMSE). These metrics provide a comprehensive evaluation of predictive performance and are defined as follows:

$$
\begin{aligned}
\text{MAPE} &= \frac{100\%}{n}\sum_{i=1}^{n}\left|\frac{I_{\text{data}}(t_i) - I_{\text{model}}(t_i)}{I_{\text{data}}(t_i)}\right|,\\
\text{RMSE} &= \sqrt{\frac{1}{n}\sum_{i=1}^{n}\left(I_{\text{data}}(t_i) - I_{\text{model}}(t_i)\right)^2}.
\end{aligned}
$$

These error metrics, given in Fig. 2, indicate a strong model fit. Additionally, a bar diagram comparing the

Table 2 Values of model parameters

Parameters	Value	Source
Λ	0.4	[67]
$\bar{\beta}$	0.8977	Fitted
μ	0.000286	[67]
ω	0.0635	Fitted
θ_1	0.1524	Fitted
θ_2	0.1935	Fitted
η_1	0.7	[68]
η_2	0.75	[68]
ϕ	0.1818	Assumed
λ	0.6276	Fitted
τ	0.2450	Fitted
ρ	0.8	Assumed
ϵ_1	0.2872	Fitted
ϵ_2	0.1635	Fitted
κ_1	0.6	Assumed
κ_2	0.2	Assumed

Table 3 Initial conditions for the model variables

	S (millions)	$V_{(i)}$ (millions)	$V_{(ii)}$ (millions)	E (millions)	I (millions)
Initial value	447	688	241	0.21	0.105

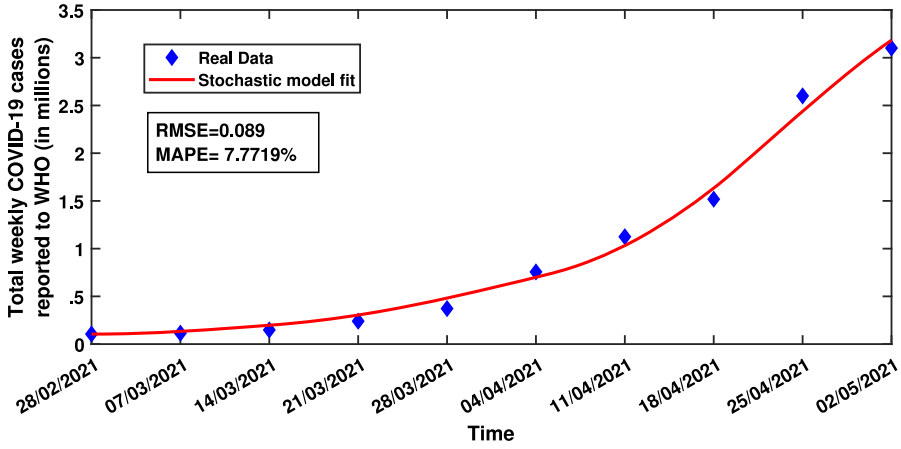

Fig. 2 Fitting of the model (3) to real data of total weekly number of COVID-19 cases in India reported to WHO using *lsqcurvefit* function in MATLAB R2023b

actual data with model predictions, as shown in Fig. 3b, highlights the close alignment between the model and the observed data, confirming the effectiveness of the model in capturing real-world dynamics and trends.

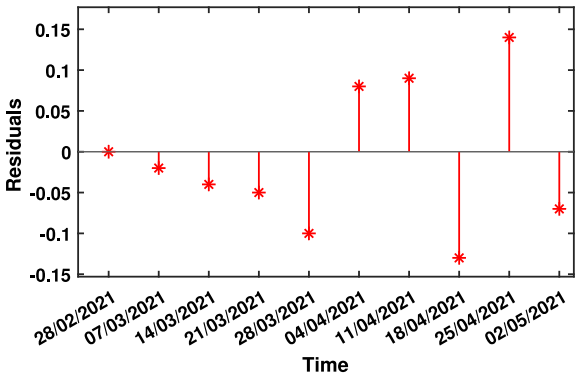

(a) Residuals of the fitting of the model (3) to real data of total weekly reported COVID-19 cases reported to WHO in India

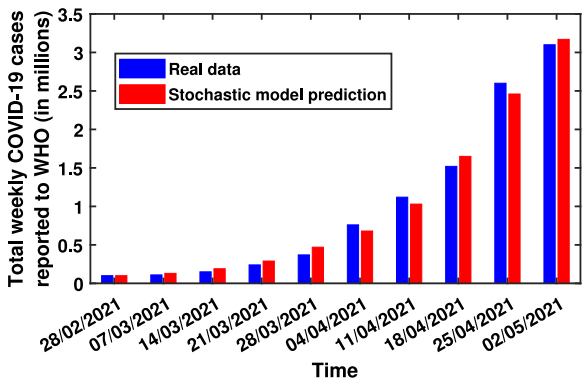

(b) Bar diagram of the fitting of the model (3) with real data from India

Fig. 3 Goodness of fit for model (3) compared to real data

$$R_0^s = \frac{\bar{\beta}\phi\left\{S^0\exp\left(\frac{\kappa_2^2}{16\kappa_1}\right) + (1-\eta_2)V_{(i)}^0\exp\left(\frac{\kappa_2^2}{12\kappa_1}\right) + (1-\eta_2)V_{(ii)}^0\exp\left(\frac{\kappa_2^2}{12\kappa_1}\right)\right\}}{(\lambda+\omega+\mu)(\phi+\tau+\mu)} = 1.1555 > 1.$$

5.2 Validation of theoretical results through numerical simulations

Validating theoretical findings through numerical simulations is crucial for ensuring the robustness and practicality of theoretical models. Numerical simulations offer a tangible method to test and confirm theoretical predictions across various conditions and scenarios that might be challenging to examine analytically. This validation process not only verifies the accuracy of theoretical results but also identifies potential limitations or assumptions, refining models for enhanced real-world applicability. In this context, we validate our theoretical findings through appropriate numerical simulations.

Firstly, we set all parameter values as specified in Table 2. Then, it can be calculated that

$$R_0^e = \sqrt{R_0^d} + \frac{\bar{\beta}\phi(S^0 + (1-\eta_1)V_{(i)} + (1-\eta_2)V_{(ii)})\left(1+\exp\left(\frac{\kappa_2^2}{4\kappa_1}\right) - 2\exp\left(\frac{\kappa_2^2}{4\kappa_1}\right)\right)}{\sqrt{R_0^d}(\phi+\tau+\mu)\min\{\phi+\tau+\mu, \lambda+\omega+\mu\}} = 0.9691 < 1.$$

According to the Theorem 4.3, we can assert that a stationary distribution exists for the solution of the model (3). This is illustrated in Fig. 4. Further, from Fig. 5, it can be observed that the solution for each compartment of the system approximately follows a normal distribution, with the mean located at the corresponding endemic equilibrium points.

Next, we change the value of θ_1 to 0.25 while keeping all other parameters as specified in Table 2. It can then be calculated that

Hence, according to Theorem 4.4, we can conclude that the infected compartment $I(t)$ and the exposed compartment $E(t)$ will become extinct from the population exponentially. The extinction behavior of the model (3) under these circumstances is demonstrated in Fig. 6.

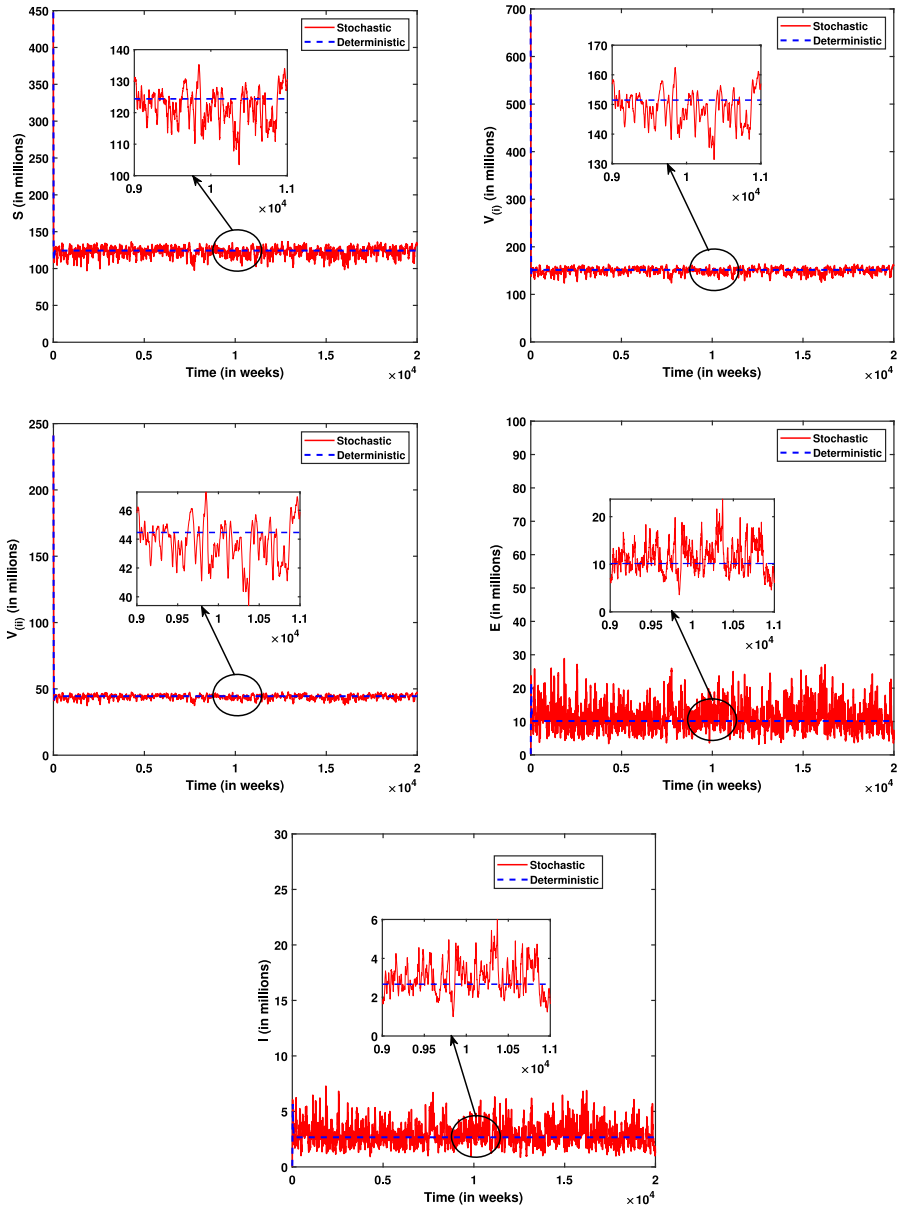

Fig. 4 Stationary behavior of the solution of the model (3) when $R_0^s = 1.1555 > 1$

We also examined the variations in the values of R_0^s and R_0^e with respect to the stochastic parameters κ_1 and κ_2 from the O-U process, as illustrated in Fig. 7. Notably, it can be observed that as the mean reversion speed increases, the values of the threshold parameters decrease. Conversely, as the noise volatility increases, the values of the stochastic threshold parameters also increase. This highlights the significant impact of the stochastic parameters on the infection thresholds, demonstrating their potential to influence the progression of the infection within the population.

5.3 Influence of key parameters on the dynamics of the COVID-19 s wave in India

Historically, the outbreak of a contagious disease in a population often follows a similar trajectory. Initially, the infection spreads slowly, affecting a small portion of the population without causing widespread alarm. However, as it continues to propagate, the number of cases rises exponentially, eventually reaching a tipping point where the outbreak starts to disrupt everyday life. At this stage, the disease impacts public health,

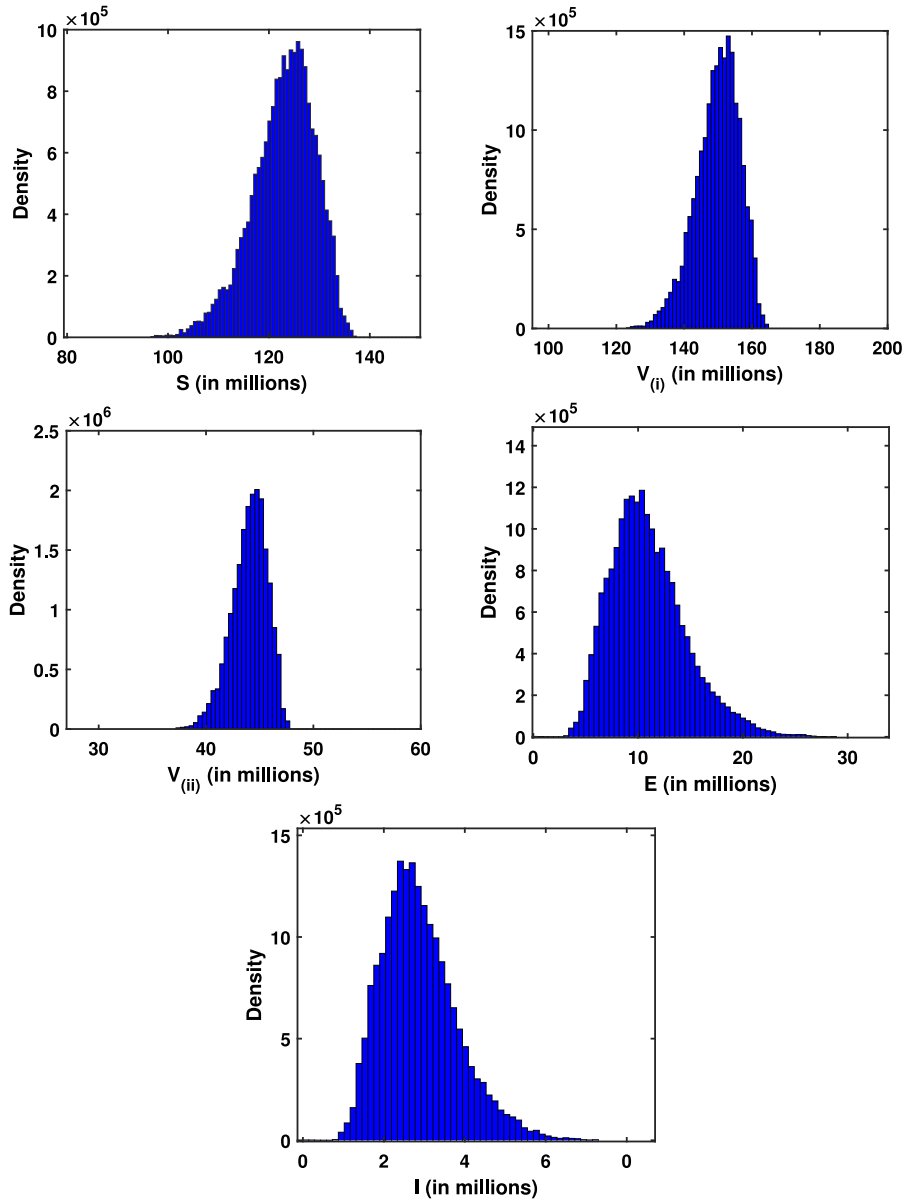

Fig. 5 Histograms of the solution of the model (3) when $R_0^s = 1.1555 > 1$

the economy and social stability, significantly affecting the ease of living of people. With increasing pressure from the public and growing strain on healthcare systems, government agencies are compelled to intervene. As the outbreak escalates, authorities implement various control measures, such as lockdowns, travel restrictions, mass testing and public health campaigns to promote preventive behaviors like hand hygiene, mask-wearing and social distancing. Vaccination programs, when available, are rolled out to boost population immunity. These interventions collectively aim to reduce the rate of transmission and slow the spread of the infection.

Over time, these control measures take effect, leading to a stagnation in the growth of new cases. The speed at which the infection spreads diminishes, and the reproduction rate drops below the critical threshold needed to sustain the outbreak. Eventually, one of two outcomes occurs: either the infection is completely eradicated, and the outbreak dies out, or the disease is brought under manageable control, allowing for a

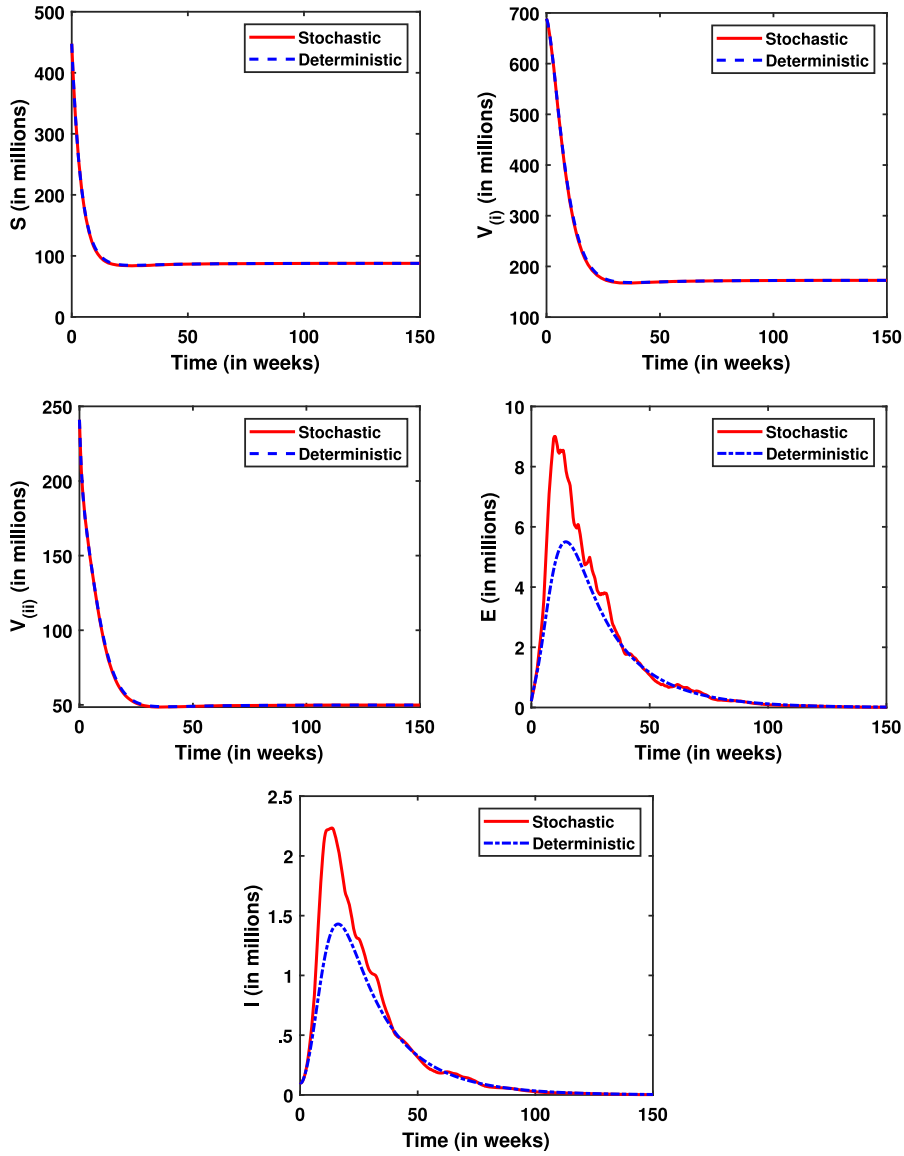

Fig. 6 Extinction dynamics of the model (3) when $R_0^e = 0.9691 < 1$

return to near-normal conditions, albeit with ongoing surveillance and occasional interventions.

The primary focus of this section is to explore how altering parameter values in the stochastic model can help further reduce and control the infection after reaching the peak of an epidemic wave. By varying these parameters within specified ranges, we aim to understand their impact on the number of affected individuals over time. This analysis seeks to identify how different scenarios influence the trajectory of the epidemic, revealing critical thresholds and ranges that can significantly modify the progression of the disease. Insights gained from this study are crucial for developing effective public health strategies and interventions, enabling policymakers and healthcare professionals to make informed, data-driven decisions to manage and mitigate future waves of COVID-19 and similar infection outbreaks.

We utilized the Partial Rank Correlation Coefficient (PRCC) method in combination with Latin Hypercube Sampling (LHS) [69] to conduct a thorough global sensitivity and uncertainty analysis of the key parameters in the model (3), namely $\bar{\beta}$, θ_1, θ_2, λ, κ_1 and κ_2. These parameters were selected because they are considered

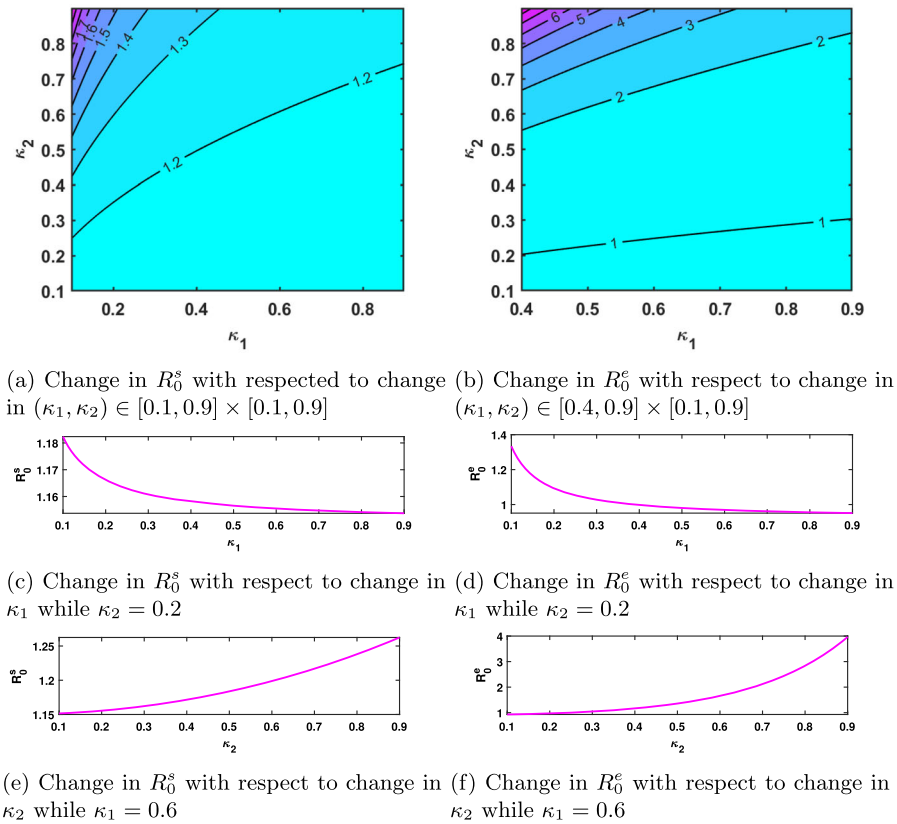

Fig. 7 Changes in the threshold parameters R_0^s and R_0^e for different values of κ_1 and κ_2

(a) Change in R_0^s with respected to change in $(\kappa_1, \kappa_2) \in [0.1, 0.9] \times [0.1, 0.9]$

(b) Change in R_0^e with respect to change in $(\kappa_1, \kappa_2) \in [0.4, 0.9] \times [0.1, 0.9]$

(c) Change in R_0^s with respect to change in κ_1 while $\kappa_2 = 0.2$

(d) Change in R_0^e with respect to change in κ_1 while $\kappa_2 = 0.2$

(e) Change in R_0^s with respect to change in κ_2 while $\kappa_1 = 0.6$

(f) Change in R_0^e with respect to change in κ_2 while $\kappa_1 = 0.6$

controllable through various government programs, while κ_1 and κ_2 are stochastic parameters. PRCC values were computed at different time points for each parameter, which allowed us to examine their varying influence throughout the simulation. This time-dependent analysis facilitates understanding how the impact of each parameter changes over time. The chosen response function in this analysis was the compartment I, representing the number of individuals infected with COVID-19. The PRCC values provide valuable information about the direction and strength of the correlation between each parameter and the response function I. Specifically, positive PRCC values indicate a direct positive correlation, while negative values suggest an inverse relationship with I. The magnitude of the PRCC values further quantifies the strength of these correlations, categorized as follows:

(i) Absolute PRCC values below 0.2 suggest that the parameter has a minimal impact on I.
(ii) Values between 0.2 and 0.4 indicate a moderate but meaningful correlation.
(iii) Values greater than 0.4 represent a strong correlation, highlighting parameters that have a significant influence on I.

This classification allows for a clear understanding of the relative importance of each parameter, facilitating their prioritization in the context of model behavior and predictions. Figure 8 represents the time-varying effects of the PRCC values of the key parameters of the stochastic model where the response function is $I(t)$.

Initially, we analyzed data from India during a critical period when a surge in COVID-19 cases was occurring. Starting on February 28, 2021, the number of infections began to rise steadily, moving from negligible levels to approximately 3 million cases by May 2, 2021, in a relatively short span. At this point, the impact of the virus became undeniable, straining public health systems and prompting authorities to implement various interventions to curb the spread. In our study, we fit our model to this specific period of the outbreak, capturing the data from the initial emergence of cases up until they reached approximately the 3 million

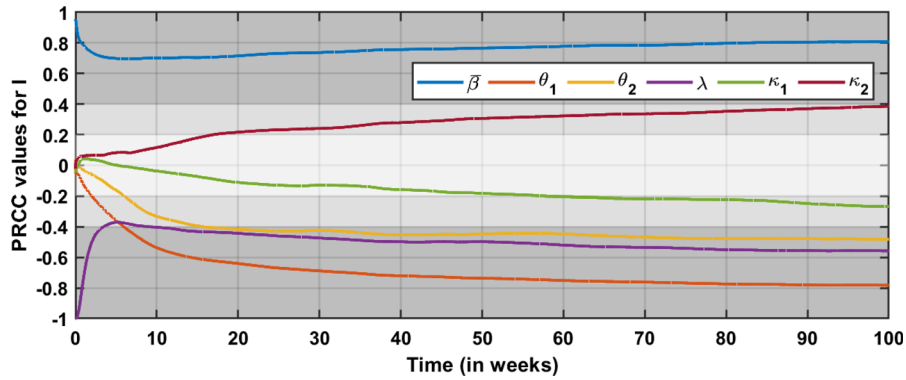

Fig. 8 The PRCC values of the key parameters in the model (3) are analyzed with $I(t)$, representing the number of COVID-19 infected individuals in the population, as the response function. The shaded regions in the plot illustrate the strength of the correlation: the dark gray area indicates PRCC values corresponding to moderate correlation, while the darker gray region represents PRCC values indicating significant correlation

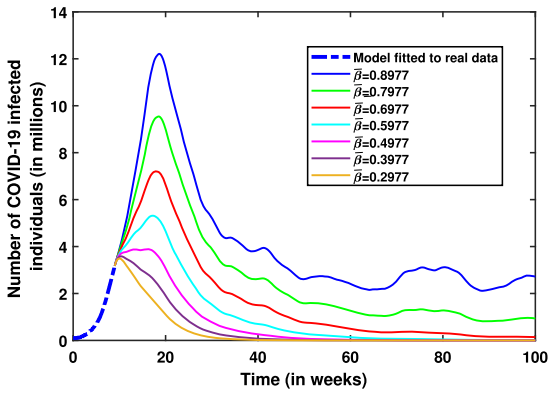

(a) Dynamical behavior for different values of $\bar{\beta}$

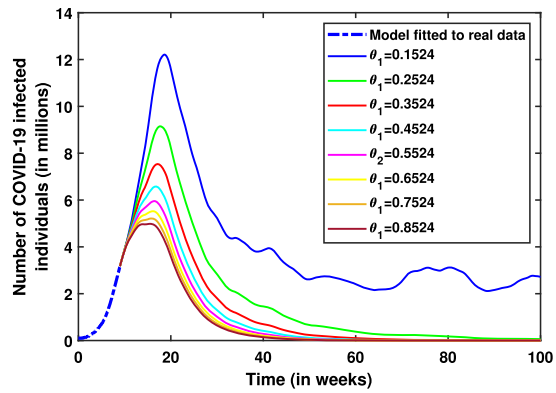

(b) Dynamical behavior for different values of θ_1

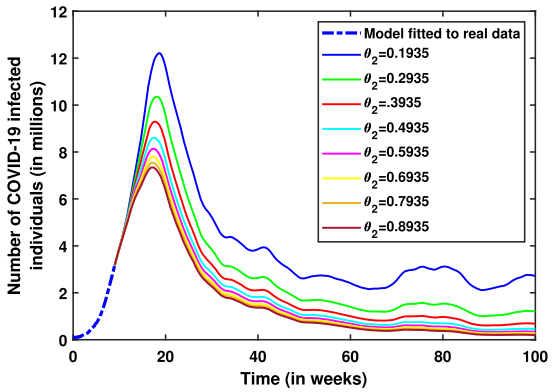

(c) Dynamical behavior for different values of θ_2

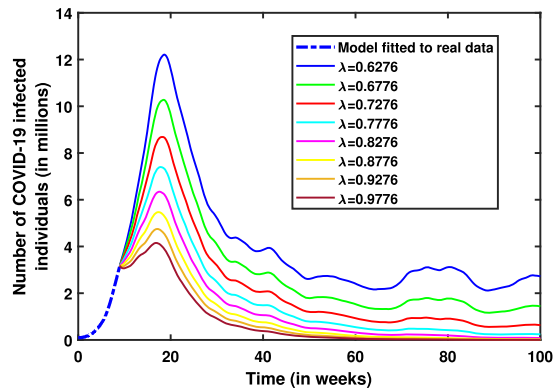

(d) Dynamical behavior for different values of λ

Fig. 9 Comparison of the dynamical behavior of the stochastic model (3) for different values of $\bar{\beta}$ (top left), θ_1 (top right), θ_2 (bottom left) and λ (bottom right)

mark. This allowed us to reflect the natural progression of the infection before significant public health measures were enforced. Our assumption is that once the infection reached a critical threshold, policymakers began introducing interventions, which led to changes in the parameter values of the model. Our study aims to identify the most effective control measures by analyzing how changes in key parameters influence the course of the pandemic. We evaluate the impact of these variations on COVID-19 case numbers, focusing on how adjustments to specific parameters can reduce the spread and inform targeted public health strategies.

In this subsection, we focus on how changes in critical factors such as the long-term mean value of the transmission rate, vaccination rates (first and second doses) and recovery rate affect both the extinction time of the infection and the size of the infection peak during a wave. By exploring various combinations of these parameters, we assess how quickly the virus could be eradicated and the potential severity of the outbreak, providing valuable insights for mitigating future waves.

5.3.1 Impact of varying long-term mean value of the transmission rate

Reducing the long-term mean value of the transmission rate significantly impacts both the peak number of cases and the extinction time of the epidemic. For instance, a modest 11% reduction in $\bar{\beta}$ results in a decrease in peak cases to 9.5452 million, but the epidemic does not reach extinction and remains endemic. A more substantial reduction of 22% lowers the peak to 7.2046 million cases and reduces the extinction time to approximately 304 weeks. Further reductions to 33%, 44% and 56% progressively decrease the peak and shorten the extinction time, highlighting a non-linear relationship between $\bar{\beta}$ and epidemic dynamics. At a 67% reduction, the peak number of cases drops to 3.4936 million, and the extinction time is significantly reduced to 34.82 weeks. This demonstrates that substantial decreases in $\bar{\beta}$ are crucial for controlling and potentially eradicating the epidemic.

5.3.2 Impact of varying first dose vaccination rate

Increasing the first dose vaccination rate markedly influences the trajectory of the epidemic. A 65.6% increase in θ_1 leads to a peak reduction to 9.1509 million cases and an extinction time of 123 weeks. Larger increases in θ_1 continue to lower both the peak number of cases and the extinction time, with a 393.5% increase resulting in peak of 5.2140 million cases and an extinction time of 39.35 weeks. These results emphasize that higher vaccination rates can effectively reduce both the severity of the epidemic and the time required for extinction, though the rate of reduction diminishes with further increases in θ_1.

5.3.3 Impact of varying second dose vaccination rate

The second dose vaccination rate also affects epidemic outcomes, but its impact on extinction time is less pronounced compared to θ_1. Increasing θ_2 by 51.6% lowers the peak number of cases to 10.3526 million, but the extinction time remains high at 1074.4 weeks. Even with substantial increases up to 393.5%, the extinction time remains lengthy, though the peak continues to decrease. For example, at a 393.5% increase, the peak reduces to 7.1817 million cases. This indicates that while increasing θ_2 can reduce peak cases, achieving a significant reduction in extinction time may require combining vaccination efforts with other public health measures.

5.3.4 Impact of varying recovery rate

Variations in the recovery rate have a notable effect on both the peak number of cases and the extinction time. Increasing λ by 16% results in a peak reduction to 8.6880 million cases and an extinction time of 331.32 weeks. Larger increases in λ lead to more significant reductions in both peak cases and extinction time, with a 55.7% increase resulting in a peak of 4.1523 million cases and an extinction time of 60.5 weeks. The diminishing returns at higher recovery rates suggest that while increasing λ is beneficial for reducing epidemic duration, additional measures may be necessary to achieve further reductions in peak cases and to manage the epidemic effectively.

In summary, the analysis reveals that reducing the long-term mean value of the transmission rate and increasing vaccination rates are critical strategies for controlling the epidemic. While higher recovery rates also contribute to a shorter epidemic duration, the combined effects of multiple strategies, including vaccination and public health measures, are essential for effective epidemic management (Figs. 9, 10, 11).

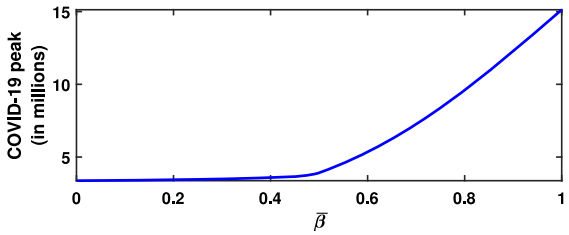

(a) Peak values for different values of $\bar{\beta}$

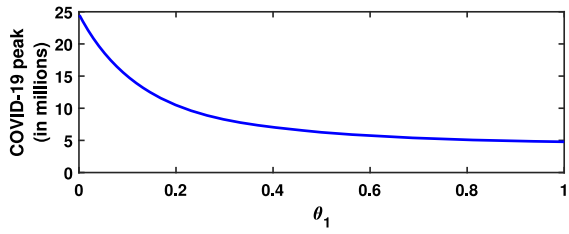

(b) Peak values for different values of θ_1

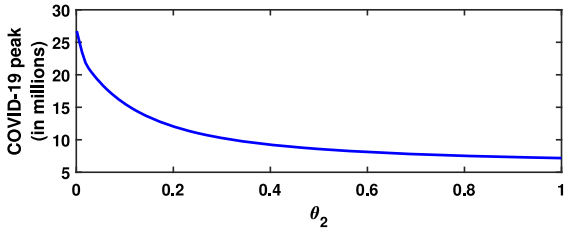

(c) Peak values for different values of θ_2

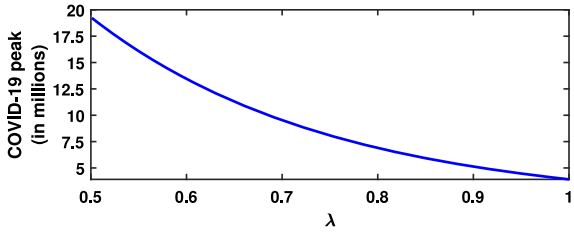

(d) Peak values for different values of λ

Fig. 10 Peak values of the stochastic model for varying parameters $\bar{\beta}$, θ_1, θ_2 and λ

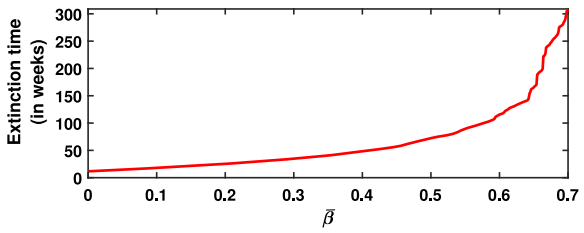

(a) Extinction time for different values of $\bar{\beta}$

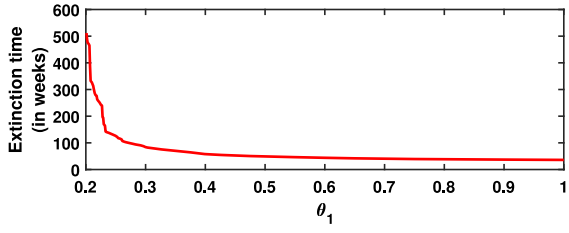

(b) Extinction time for different values of θ_1

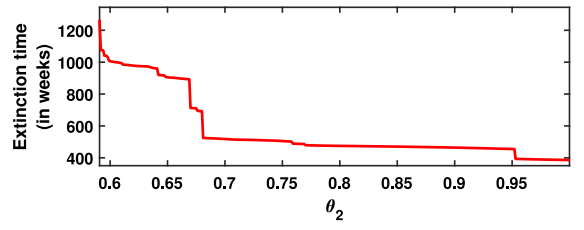

(c) Extinction time for different values of θ_2

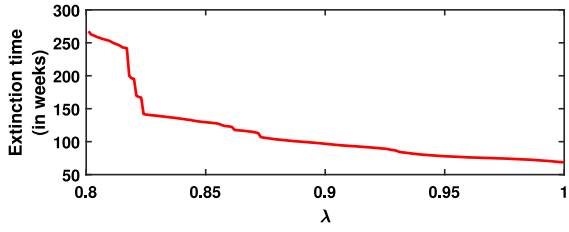

(d) Extinction time for different values of λ

Fig. 11 Extinction times of the stochastic model for varying parameters $\bar{\beta}$, θ_1, θ_2 and λ

5.4 Impact of varying parameters of Ornstein-Uhlenbeck process

In this subsection, we examine the influence of different parameters of the O-U process on the dynamics of COVID-19 infection peaks in India. Specifically, we focus on two critical parameters of the O-U process: the mean reversion speed κ_1 and the noise volatility κ_2. These parameters play pivotal roles in determining the behavior of the infection dynamics, reflecting both the rate at which the infection levels revert to their long-term mean and the extent of randomness in the infection process.

By examining these parameters, we aim to gain a deeper understanding of the stochastic behavior of the COVID-19 epidemic and derive actionable insights for public health strategies. The results from these analyses are intended to inform policymakers about the potential implications of stochastic parameter adjustments on epidemic control measures and to enhance our ability to predict and manage future outbreaks. The following analysis provide a detailed understanding of how varying κ_1 and κ_2 affects peak infection sizes, supported by empirical data and visual representations.

5.4.1 Impact of varying mean reversion speed κ_1

In this subsection, we investigate the impact of varying the mean reversion speed κ_1 on the peak size of COVID-19 cases in India. The parameter κ_1 is crucial in determining how rapidly the infection dynamics revert to their long-term mean, reflecting the effectiveness of interventions such as vaccination and social distancing measures.

To understand the influence of κ_1, we evaluated the COVID-19 peak infection size for six different values of κ_1 (0.15, 0.30, 0.45, 0.60, 0.75 and 0.90), with the baseline reference value set at $\kappa_1 = 0.60$. The peak infection size, measured in millions of cases, is calculated for all these values. The stochastic threshold parameter R_0^s was found to be greater than 1 for all values of κ_1, indicating that the infection would persist in the population over the long term. This persistence demonstrates the stationary behavior of the process, which is why the extinction time of the infection is not analyzed. On the otherhand, the dynamic hevaior of the infection compartment for different values of κ_1 is demonstrated in Fig. 12a. Further, the size of the COVID-19 peaks for varyig values of κ_1 from 0 to 1 is presented in Fig. 12c.

As shown in the Table 4, there is a clear inverse relationship between κ_1 and the peak infection size. When κ_1 increases, the peak size decreases. For instance, a low κ_1 of 0.15 results in a peak infection size of 19.6223 million, representing a 60.61% increase compared to the baseline value of 12.2132 million at $\kappa_1 = 0.60$. Conversely, increasing κ_1 to 0.90 reduces the peak size to 10.8938 million, a decrease of 10.80% from the baseline. This inverse relationship suggests that a higher κ_1 leads to more rapid stabilization of infection levels following any disturbances, such as the emergence of new variants or the relaxation of public health measures. This stabilization could be due to a more effective public health response, including faster vaccine distribution, more stringent adherence to preventive measures, rigorous enforcement of social distancing, or other interventions that reduce the spread of the virus more effectively. For policymakers, these insights suggest that strategies aimed at increasing κ_1 could be instrumental in controlling the severity of future epidemic waves. In practice, this could involve optimizing the timing and intensity of interventions to maximize their impact on the infection dynamics, thereby reducing the strain on healthcare systems and minimizing the overall burden of the pandemic.

5.4.2 Impact of varying noise volatility κ_2

In this subsection, we explore the effect of varying noise volatility κ_2 on the peak size of COVID-19 cases in India. The parameter κ_2 captures the randomness and uncertainty in the infection dynamics, and its impact on the peak infection size when an outbreak happens in the region. This analysis provides valuable insights into how fluctuations in infection rates might influence the overall burden of the epidemic.

To assess the impact of κ_2, we analyzed the peak infection size for eight different values of κ_2 ranging from 0.1 to 0.8. The baseline reference value was set at $\kappa_2 = 0.2$, with the corresponding peak infection size recorded as 12.2132 million cases. The results for different κ_2 values are summarized below. Here also, the stochastic threshold parameter R_0^s was found to be greater than 1 for all values of κ_2, ensuring the persistence of infection over time. The dynamic behavior of the infection compartment for various κ_2 values is depicted in Fig. 12b. Additionally, the peak sizes of COVID-19 cases for different κ_2 values are shown in Fig. 12d.

As shown in Table 5, there is a distinct positive correlation between κ_2 and the peak infection size. Increasing κ_2 results in a notable rise in the peak infection size. For example, a lower κ_2 value of 0.1 yields a peak infection size of 10.0368 million, which is a 17.97% decrease compared to the baseline peak of 12.2132 million at $\kappa_2 = 0.2$. On the other hand, when κ_2 is increased to 0.8, the peak infection size escalates to 35.0272 million, reflecting a 187.7% increase from the baseline. This positive trend demonstrates that higher noise volatility is associated with more pronounced peaks in infection rates. The growing randomness in

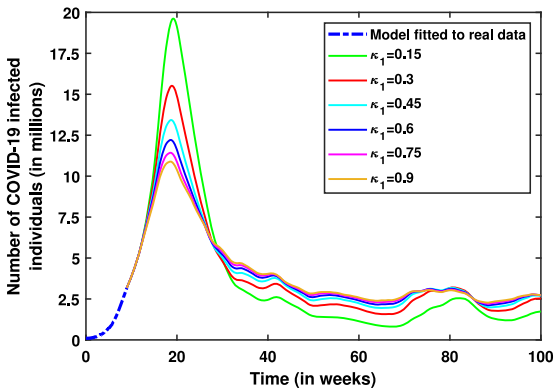

(a) Dynamical behavior for different values of κ_1

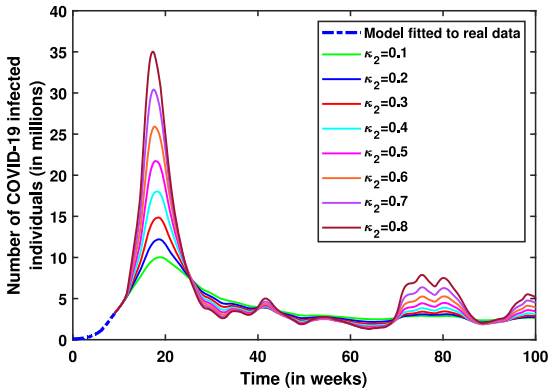

(b) Dynamical behavior for different values of κ_2

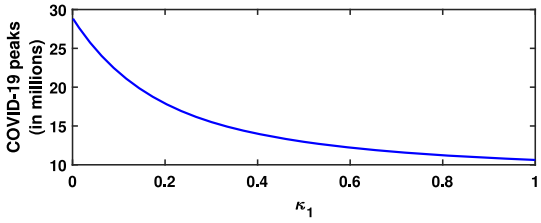

(c) Peak values for varying κ_1

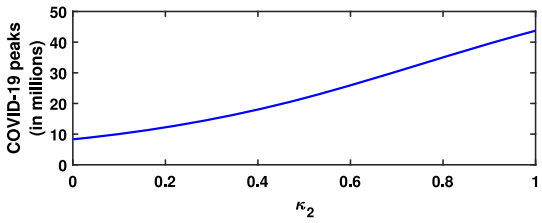

(d) Peak values for varying κ_2

Fig. 12 Comparison of the dynamical behavior (top row) and peak values (bottom row) of the stochastic model (3) for different values of κ_1 (left column) and κ_2 (right column)

Table 4 Effect of κ_1 on peak infection size

κ_1	Peak infection size (in millions)	Percentage change from baseline (%)
0.1500	19.6223	+60.61
0.3000	15.5191	+27.01
0.4500	13.4311	+9.97
0.6000 (Baseline)	12.2132	0.00
0.7500	11.4316	−6.40
0.9000	10.8938	−10.80

infection dynamics with increasing κ_2 leads to more significant peaks, indicating a broader spread of the virus during epidemic waves. This finding emphasizes the necessity of incorporating stochastic variability into epidemic predictions and underscores the importance of adaptable public health strategies. Policymakers should focus on managing infection volatility to control peak sizes effectively. Approaches such as optimizing vaccine distribution, adjusting social distancing protocols and bolstering surveillance systems are crucial for mitigating the effects of future epidemic waves and better managing infection dynamics.

6 Conclusion and future direction

The COVID-19 pandemic, caused by SARS-CoV-2 virus, has profoundly affected global health, economics and daily life. Since its emergence, multiple waves of infection have prompted extensive research into understanding its transmission dynamics and developing mit-

Table 5 Effect of κ_2 on peak infection size

κ_2	Peak infection size (in millions)	Percentage change from baseline (%)
0.1000	10.0368	−17.97
0.2000 (Baseline)	12.2132	0.00
0.3000	14.8674	+21.76
0.4000	18.0205	+47.55
0.5000	21.7275	+78.27
0.6000	25.9184	+112.37
0.7000	30.4176	+149.6
0.8000	35.0272	+187.7

igation strategies. Vaccines have played a crucial role in controlling the virus, yet predicting vaccination outcomes and new outbreaks remains challenging. In this study, we developed a stochastic model to analyze the transmission dynamics of SARS-CoV-2 in India, incorporating dual vaccine doses using a logarithmic mean-reverting O-U process. The key findings of this study are summarized as follows:

(i) We developed a deterministic system that classifies individuals into distinct compartments: those who received only the first dose and those who completed both doses, along with compartments for susceptible, exposed, infected and recovered stages. This system was rigorously analyzed mathematically by:
   - Establishing the existence and uniqueness of a global positive solution, which is bounded.
   - Deriving the disease-free equilibrium points.
   - Calculating the basic reproduction number (R_0^d).
   - Demonstrating that the disease-free equilibrium point is locally asymptotically stable when $R_0^d < 1$.

(ii) We extended the deterministic model into a stochastic framework by incorporating perturbations to the key parameter, β (the COVID-19 transmission rate), modeled using a stochastic differential equation governed by the Ornstein-Uhlenbeck (O-U) process.

(iii) The mathematical and biological soundness of the stochastic model was thoroughly investigated through the careful selection of Lyapunov functions. Specifically:
   (i) A positive invariant set was defined as:
   $$\Theta = \left\{(b, S, V_{(i)}, V_{(ii)}, E, I) \in \mathbb{R}_+^5 \times \mathbb{R} : S < S^0, V_{(i)} < V_{(i)}^0, V_{(ii)} < V_{(ii)}^0, A < \frac{\Lambda}{\mu}\right\},$$
   ensuring the existence of a unique global positive and bounded solution.
   (ii) We derived a stochastic threshold parameter, R_0^s, which ensures the persistence of the disease over an extended period when $R_0^s > 1$.
   (iii) Another stochastic threshold parameter, R_0^e, was calculated, indicating that the infection will die out exponentially when $R_0^e < 1$.

(iv) The model was fitted to real-world data from India during the second COVID-19 wave. Using the $lsqcurvefit$ function in MATLAB R2023b, region-specific parameter values were estimated, reflecting the outbreak scenario. The model demonstrated an excellent fit to the data, with very low error values (RMSE = 0.089, MAPE = 7.7719%).

(v) We performed a global sensitivity analysis to identify key controllable parameters affecting the behavior of the model. The analysis employed the partial rank correlation coefficient (PRCC) method and Latin hypercube sampling (LHS). Key parameters with significant influence on the number of infected individuals included $\bar{\beta}$ (approximate PRCC value - 0.8), θ_1 (approximate PRCC value - −0.8), θ_2 (approximate PRCC value - −0.5), λ (approximate PRCC value - −0.6), κ_1 (approximate PRCC value - −0.2) and κ_2 (approximate PRCC value - 0.4).

(vi) To provide actionable insights, we examined scenarios where government authorities might imple-

ment control measures during the progression of epidemic. By adjusting parameters, we explored outcomes such as extinction time and infection peak size. This analysis offers valuable guidance for managing future outbreaks by demonstrating how different intervention strategies impact the course of the epidemic.

The analysis highlights the necessity of a comprehensive, multi-faceted approach to managing and mitigating future COVID-19 waves. Central to this strategy is the reduction of the long-term mean value of the transmission rate ($\bar{\beta}$), which can be achieved through stringent public health interventions such as social distancing, mask mandates and limiting large gatherings, coupled with robust contact tracing and isolation protocols. These measures, when effectively implemented, play a critical role in lowering the peak number of cases and accelerating the extinction of the epidemic. Alongside these efforts, increasing vaccination rates, particularly for the first dose (θ_1), is pivotal in altering the trajectory of the epidemic. Accelerated vaccination campaigns, which expand access through more sites and targeted outreach, can significantly reduce peak cases and shorten the time to epidemic extinction. Ensuring that individuals complete their vaccination schedule by receiving the second dose (θ_2) is equally crucial for establishing long-term immunity and preventing severe outcomes. Moreover, enhancing the recovery rate (λ) by strengthening healthcare systems through increased hospital capacity, timely treatment and the availability of medical resources further reduces the duration and severity of the epidemic. In addition to these direct interventions, managing stochastic variability in infection dynamics, represented by mean reversion speed (κ_1) and noise volatility (κ_2), is essential for controlling unpredictable fluctuations in infection rates. Adaptive public health policies that can quickly respond to emerging variants or changes in infection patterns, supported by enhanced surveillance systems and predictive modeling, are crucial for stabilizing infection levels. Thus, an integrated approach that combines reduced transmission, increased vaccination, improved recovery rates and effective management of stochastic variability forms a robust framework for controlling and potentially eradicating COVID-19 waves. Furthermore, sustained public engagement and clear communication from health authorities are vital for ensuring compliance with these measures. By fostering public trust and emphasizing the collective benefits of these strategies, authorities can achieve the necessary levels of adherence, making this comprehensive approach not only effective in addressing the current pandemic but also in building resilience against future public health crises.

Our study has some limitations that facilitates further exploration. Epidemic model parameters often vary over time or follow periodic patterns due to environmental and seasonal changes. Future research could enhance stochastic epidemic models by incorporating more than one periodic parameter or discrete Markov switching, driven by the mean-reverting O-U process. Additionally, unlike deterministic models with a single threshold parameter, our study introduces two thresholds: R_0^e (indicating extinction if $R_0^e < 1$) and R_0^s (indicating a stationary solution if $R_0^s > 1$). However, the scenario where $R_0^e > 1$ and $R_0^s < 1$ remains unaddressed and is left for future work. Further, the model could be extended to account for emerging virus variants with different transmission dynamics and vaccine interactions. Also, incorporating heterogeneous population structures, such as age groups, urban versus rural settings, or regional disparities in healthcare access, could yield more detailed insights. Future research could explore these aspects of infection dynamics modeling.

Acknowledgements The authors express their gratitude to Faculty of Education, Phuket Rajabhat University, Thailand, for the invaluable support to the International Students Project Programme 2024.

Author contributions T. A. Midhun: Conceptualization, Formal analysis, Methodology, Software, Validation, Investigation, Writing- Original Draft, Writing- Review & Editing. S.A. Jose: Conceptualization, Formal analysis, Methodology, Validation, Investigation, Supervision, Writing- Review & Editing, Project administration. K. Murugesan: Methodology, Investigation, validation, Writing- Review & Editing. A. Jirawattanapanit: Validation, Investigation, Supervision, Writing- Review & Editing, funding acquisition, Project administration.

Funding The authors have not disclosed any funding.

Data Availability Statement No datasets were generated or analysed during the current study.

Declarations

Conflict of interest The authors declare no potential conflict of interest.

References

1. Zhu, N., Zhang, D., Wang, W., Li, X., Yang, B., Song, J., Zhao, X., Huang, B., Shi, W., Lu, R., et al.: A novel coronavirus from patients with pneumonia in China, 2019. N. Engl. J. Med. **382**(8), 727–733 (2020). https://doi.org/10.1056/NEJMoa2001017
2. Huang, C., Wang, Y., Li, X., Ren, L., Zhao, J., Hu, Y., Zhang, L., Fan, G., Xu, J., Gu, X., et al.: Clinical features of patients infected with 2019 novel coronavirus in Wuhan, China. The lancet **395**(10223), 497–506 (2020). https://doi.org/10.1016/S0140-6736(20)30183-5
3. Zhou, F., Yu, T., Du, R., Fan, G., Liu, Y., Liu, Z., Xiang, J., Wang, Y., Song, B., Gu, X., et al.: Clinical course and risk factors for mortality of adult inpatients with COVID-19 in Wuhan, China: a retrospective cohort study. The lancet **395**(10229), 1054–1062 (2020). https://doi.org/10.1016/S0140-6736(20)30566-3
4. World Health Organization, Coronavirus disease (COVID-19) pandemic, https://www.who.int/emergencies/diseases/novel-coronavirus-2019 (2020)
5. Johns Hopkins University, Coronavirus Resource Center, https://coronavirus.jhu.edu/map.html (2021)
6. International Monetary Fund, World Economic Outlook: Recovery During a Pandemic, International Monetary Fund (2021)
7. Guan, W.-J., Ni, Z.-Y., Hu, Y., Liang, W.-H., Ou, C.-Q., He, J.-X., Liu, L., Shan, H., Lei, C.-L., Hui, D.S., et al.: Clinical characteristics of coronavirus disease 2019 in China. N. Engl. J. Med. **382**(18), 1708–1720 (2020). https://doi.org/10.1056/NEJMoa2002032
8. Ministry of Health and Family Welfare, Government of India, COVID-19 Dashboard, https://mohfw.gov.in/ (2021)
9. Kapoor, M., Nidhi Kaur, K., Saeed, S., Shannawaz, M., Chandra, A.: Impact of COVID-19 on healthcare system in India: A systematic review. J. Public Health Res. **12**(3), 22799036231186348 (2023). https://doi.org/10.1177/22799036231186349
10. Voysey, M., Clemens, S.A.C., Madhi, S.A., Weckx, L.Y., Folegatti, P.M., Aley, P.K., Angus, B., Baillie, V.L., Barnabas, S.L., Bhorat, Q.E., et al.: Safety and Efficacy of the ChAdOx1 nCoV-19 Vaccine (AZD1222) against SARS-CoV-2: An Interim Analysis of Four Randomised Controlled Trials in Brazil, South Africa, and the UK. The Lancet **397**(10269), 99–111 (2021). https://doi.org/10.1016/S0140-6736(20)32661-1
11. Ella, R., Reddy, S.P., Jogdand, H., Sarangi, V., Ganneru, B., Prasad, S., Das, D., Raju, D., Praturi, U., Sapkal, G., et al.: Efficacy, Safety, and Lot-to-Lot Immunogenicity of an Inactivated SARS-CoV-2 Vaccine (BBV152): A Double-Blind, Randomised, Controlled Phase 3 Trial. The Lancet **398**(10317), 2173–2184 (2021). https://doi.org/10.1016/S0140-6736(21)02000-6
12. Logunov, D.Y., Dolzhikova, I.V., Shcheblyakov, D.V., Tukhvatulin, A.I., Zubkova, O.V., Dzharullaeva, A.S., Kovyrshina, A.V., Lubenets, N.L., Grousova, D.M., Erokhova, A.S., et al.: Safety and Efficacy of an rAd26 and rAd5 Vector-Based Heterologous Prime-Boost COVID-19 Vaccine: An Interim Analysis of a Randomised Controlled Phase 3 Trial in Russia. The Lancet **397**(10275), 671–681 (2021). https://doi.org/10.1016/S0140-6736(21)00234-8
13. Mahroug, F., Bentout, S.: Dynamics of a diffusion dispersal viral epidemic model with age infection in a spatially heterogeneous environment with general nonlinear function. Math. Methods Appl. Sci. **46**(14), 14983–15010 (2023). https://doi.org/10.1002/mma.9357
14. Djilali, S., Chen, Y., Bentout, S.: Dynamics of a delayed nonlocal reaction-diffusion heroin epidemic model in a heterogenous environment. Math. Methods Appl. Sci. (2024). https://doi.org/10.1002/mma.10327
15. Soufiane, B., Touaoula, T.M.: Global analysis of an infection age model with a class of nonlinear incidence rates. J. Math. Anal. Appl. **434**(2), 1211–1239 (2016). https://doi.org/10.1016/j.jmaa.2015.09.066
16. Djilali, S., Bentout, S., Tridane, A.: Dynamics of a generalized nonlocal dispersion SIS epidemic model. J. Evol. Equ. **24**(4), 1–24 (2024). https://doi.org/10.1007/s00028-024-01013-1
17. Bentout, S., Djilali, S.: Asymptotic profiles of a nonlocal dispersal SIR epidemic model with treat-age in a heterogeneous environment. Math. Comput. Simul. **203**, 926–956 (2023). https://doi.org/10.1016/j.matcom.2022.07.020
18. Bentout, S.: Analysis of global behavior in an age-structured epidemic model with nonlocal dispersal and distributed delay. Math. Methods Appl. Sci. **47**(9), 7219–7242 (2024). https://doi.org/10.1002/mma.9969
19. Bentout, S., Djilali, S.: Asymptotic profiles of a generalized reaction-diffusion sis epidemic model with spatial heterogeneity. Z. Angew. Math. Phys. **75**(6), 1–31 (2024). https://doi.org/10.1007/s00033-024-02373-x
20. Nastasi, G., Perrone, C., Taffara, S., Vitanza, G.: A time-delayed deterministic model for the spread of COVID-19 with calibration on a real dataset. Mathematics **10**(4), 661 (2022). https://doi.org/10.3390/math10040661
21. Yang, B., Yu, Z., Cai, Y.: The impact of vaccination on the spread of COVID-19: Studying by a mathematical model. Physica A **590**, 126717 (2022). https://doi.org/10.1016/j.physa.2021.126717
22. Diagne, M., Rwezaura, H., Tchoumi, S., Tchuenche, J.: A mathematical model of COVID-19 with vaccination and treatment. Comput. Math. Methods Med. **2021**(1), 1250129 (2021). https://doi.org/10.1155/2021/1250129
23. Paul, J.N., Mbalawata, I.S., Mirau, S.S., Masandawa, L.: Mathematical modeling of vaccination as a control measure of stress to fight COVID-19 infections. Chaos, Solitons & Fractals **166**, 112920 (2023). https://doi.org/10.1016/j.chaos.2022.112920
24. Angeli, M., Neofotistos, G., Mattheakis, M., Kaxiras, E.: Modeling the effect of the vaccination campaign on the COVID-19. Chaos, Solitons & Fractals **154**, 111621 (2022). https://doi.org/10.1016/j.chaos.2021.111621
25. Zhai, S., Luo, G., Huang, T., Wang, X., Tao, J., Zhou, P.: Vaccination control of an epidemic model with time delay and its application to COVID-19. Nonlinear Dyn. **106**(2), 1279–1292 (2021). https://doi.org/10.1007/s11071-021-06533-w
26. Omede, B.I., Jose, S.A., Anuwat, J., Park, T.: Mathematical analysis on the transmission dynamics of delta and omicron variants of COVID-19 in the United States. Model. Earth Syst. Environ. (2024). https://doi.org/10.1007/s40808-024-02101-4

27. Thomas, R., Jose, S.A., Raja, R., Alzabut, J., Cao, J., Balas, V.E.: Modeling and analysis of SEIRS epidemic models using homotopy perturbation method: A special outlook to 2019-nCoV in India. Int. J. Biomath. **15**(08), 2250059 (2022). https://doi.org/10.1142/S1793524522500590
28. Jose, S.A., Panigoro, H.S., Jirawattanapanit, A., Omede, B.I., Yaagoub, Z., et al.: Understanding COVID-19 propagation: a comprehensive mathematical model with Caputo fractional derivatives for Thailand. Front. Appl. Math. Stat. **10**, 1374721 (2024). https://doi.org/10.3389/fams.2024.1374721
29. Foy, B.H., Wahl, B., Mehta, K., Shet, A., Menon, G.I., Britto, C.: Comparing COVID-19 vaccine allocation strategies in India: A mathematical modelling study. Int. J. Infect. Dis. **103**, 431–438 (2021). https://doi.org/10.1016/j.ijid.2020.12.075
30. Biswas, S.K., Ghosh, J.K., Sarkar, S., Ghosh, U.: Covid-19 pandemic in India: a mathematical model study. Nonlinear Dyn. **102**, 537–553 (2020). https://doi.org/10.1007/s11071-020-05958-z
31. Samui, P., Mondal, J., Khajanchi, S.: A mathematical model for covid-19 transmission dynamics with a case study of India. Chaos, Solitons & Fractals **140**, 110173 (2020). https://doi.org/10.1016/j.chaos.2020.110173
32. Ambikapathy, B., Krishnamurthy, K., et al.: Mathematical modelling to assess the impact of lockdown on covid-19 transmission in India: model development and validation. JMIR Public Health Surveill. **6**(2), e19368 (2020). https://doi.org/10.2196/19368
33. Sobral, M.F.F., Duarte, G.B., da Penha Sobral, A.I.G., Marinho, M.L.M., de Souza Melo, A.: Association between climate variables and global transmission oF SARS-CoV-2. Sci. Total Environ. **729**, 138997 (2020). https://doi.org/10.1016/j.scitotenv.2020.138997
34. Singh, A., Arquam, M.: Epidemiological modeling for covid-19 spread in India with the effect of testing. Physica A **592**, 126774 (2022). https://doi.org/10.1016/j.physa.2021.126774
35. Plante, J.A., Liu, Y., Liu, J., Xia, H., Johnson, B.A., Lokugamage, K.G., Zhang, X., Muruato, A.E., Zou, J., Fontes-Garfias, C.R., et al.: Spike mutation d614g alters sars-cov-2 fitness. Nature **592**(7852), 116–121 (2021). https://doi.org/10.1038/s41586-020-2895-3
36. Zhao, J., Yuan, Q., Wang, H., Liu, W., Liao, X., Su, Y., Wang, X., Yuan, J., Li, T., Li, J., et al.: Antibody responses to sars-cov-2 in patients with novel coronavirus disease 2019. Clin. Infect. Dis. **71**(16), 2027–2034 (2020). https://doi.org/10.1093/cid/ciaa344
37. Allen, L.J.: An Introduction to Stochastic Epidemic Models. Springer, Berlin (2008)
38. Din, A., Li, Y.: Optimizing HIV/AIDS dynamics: stochastic control strategies with education and treatment. Eur. Phys. J. Plus **139**(9), 812 (2024). https://doi.org/10.1140/epjp/s13360-024-05605-1
39. Din, A.: Bifurcation analysis of a delayed stochastic HBV epidemic model: Cell-to-cell transmission. Chaos, Solitons & Fractals **181**, 114714 (2024). https://doi.org/10.1016/j.chaos.2024.114714
40. Ain, Q.T.: Nonlinear stochastic cholera epidemic model under the influence of noise. J. Math. Tech. Model. **1**(1), 52–74 (2024). https://doi.org/10.56868/jmtm.v1i1.30
41. Shah, S.M.A., Tahir, H., Khan, A., Arshad, A., et al.: Stochastic model on the transmission of worms in wireless sensor network. J. Math. Tech. Model. **1**(1), 75–88 (2024). https://doi.org/10.56868/jmtm.v1i1.31
42. Khan, T., Zaman, G., El-Khatib, Y.: Modeling the dynamics of novel coronavirus (COVID-19) via stochastic epidemic model. Res. Phys. **24**, 104004 (2021). https://doi.org/10.1016/j.rinp.2021.104004
43. Hwang, K.K., Edholm, C.J., Saucedo, O., Allen, L.J., Shakiba, N.: A hybrid epidemic model to explore stochasticity in COVID-19 dynamics. Bull. Math. Biol. **84**(9), 91 (2022). https://doi.org/10.1007/s11538-022-01030-6
44. Adak, D., Majumder, A., Bairagi, N.: Mathematical perspective of COVID-19 pandemic: Disease extinction criteria in deterministic and stochastic models. Chaos, Solitons & Fractals **142**, 110381 (2021). https://doi.org/10.1016/j.chaos.2020.110381
45. Li, Y., Wei, Z.: Dynamics and optimal control of a stochastic coronavirus (COVID-19) epidemic model with diffusion. Nonlinear Dyn. (2022). https://doi.org/10.1007/s11071-021-06998-9
46. Omame, A., Abbas, M., Baleanu, D.: A stochastic model to assess the epidemiological impact of vaccine booster doses on covid-19 and viral hepatitis b co-dynamics with real data. CMES-Comput. Model. Eng. Sci. **138**, 2973–3012 (2023). https://doi.org/10.32604/cmes.2023.029681
47. Aalen, O.O., Gjessing, H.K.: Survival models based on the Ornstein-Uhlenbeck process. Lifetime Data Anal. **10**, 407–423 (2004). https://doi.org/10.1007/s10985-004-4775-9
48. Lipsitch, M., Donnelly, C.A., Fraser, C., Blake, I.M., Cori, A., Dorigatti, I., Ferguson, N.M., Garske, T., Mills, H.L., Riley, S., et al.: Potential biases in estimating absolute and relative case-fatality risks during outbreaks. PLoS Negl. Trop. Dis. **9**(7), e0003846 (2015). https://doi.org/10.1371/journal.pntd.0003846
49. Korber, B., Fischer, W.M., Gnanakaran, S., Yoon, H., Theiler, J., Abfalterer, W., Hengartner, N., Giorgi, E.E., Bhattacharya, T., Foley, B., et al.: Tracking changes in sars-cov-2 spike: evidence that d614g increases infectivity of the covid-19 virus. Cell **182**(4), 812–827 (2020). https://doi.org/10.1016/j.cell.2020.06.043
50. Allen, L.J.: A primer on stochastic epidemic models: formulation, numerical simulation, and analysis. Infect. Dis. Model. **2**(2), 128–142 (2017). https://doi.org/10.1016/j.idm.2017.03.001
51. Hansen, T.F.: Stabilizing selection and the comparative analysis of adaptation. Evolution **51**(5), 1341–1351 (1997). https://doi.org/10.1111/j.1558-5646.1997.tb01457.x
52. Uhlenbeck, G.E., Ornstein, L.S.: On the theory of the Brownian motion. Phys. Rev. **36**(5), 823 (1930). https://doi.org/10.1103/PhysRev.36.823
53. Allen, E.: Environmental variability and mean-reverting processes. Discrete Contin. Dyn. Syst. Ser. B **21**(7), 2073–2089 (2016). https://doi.org/10.3934/dcdsb.2016037
54. Zhang, X., Zhang, X.: Threshold behaviors and density function of a stochastic parasite-host epidemic model with Ornstein-Uhlenbeck process. Appl. Math. Lett. **153**, 109079 (2024). https://doi.org/10.1016/j.aml.2024.109079
55. Liu, Q.: Stationary distribution and extinction of a stochastic HLIV model with viral production and Ornstein-Uhlenbeck process. Commun. Nonlinear Sci. Numer. Simul.

119, 107111 (2023). https://doi.org/10.1016/j.cnsns.2023.107111
56. Shi, Z., Jiang, D., Fu, J.: Stochastic dual epidemic hypothesis model with Ornstein-Uhlenbeck process: analysis and numerical simulations with SARS-CoV-2 variants. J. Math. Anal. Appl. **535**(2), 128232 (2024). https://doi.org/10.1016/j.jmaa.2024.128232
57. Su, T., Zhang, X., Jiang, D.: Dynamic analysis of generalized epidemic models with latent period, quarantine, governmental intervention and Ornstein-Uhlenbeck process. Nonlinear Dyn. **112**(9), 7749–7770 (2024). https://doi.org/10.1007/s11071-024-09458-2
58. Su, X., Zhang, X., Jiang, D.: Dynamics of a stochastic HBV infection model with general incidence rate, cell-to-cell transmission, immune response and Ornstein-Uhlenbeck process. Chaos, Solitons & Fractals **186**, 115208 (2024). https://doi.org/10.1016/j.chaos.2024.115208
59. Bagcchi, S.: The world's largest COVID-19 vaccination campaign, The Lancet. Infect. Dis. **21**(3), 323 (2021)
60. Mao, X.: Stochastic Differential Equations and Applications. Elsevier, Amsterdam (2007)
61. Shi, Z., Jiang, D.: A viral co-infection model with general infection rate in deterministic and stochastic environments. Commun. Nonlinear Sci. Numer. Simul. **126**, 107436 (2023). https://doi.org/10.1016/j.cnsns.2023.107436
62. Yang, X., Chen, L., Chen, J.: Permanence and positive periodic solution for the single-species nonautonomous delay diffusive models. Comput. Math. Appl. **32**(4), 109–116 (1996). https://doi.org/10.1016/0898-1221(96)00129-0
63. Shi, Z., Jiang, D.: Unveiling measles transmission dynamics: Insights from a stochastic model with nonlinear incidence. Stud. Appl. Math. **152**(4), 1077–1109 (2024). https://doi.org/10.1111/sapm.12670
64. Berman, A., Plemmons, R.J.: Nonnegative matrices in the mathematical sciences, SIAM, (1994)
65. Higham, D.J.: An algorithmic introduction to numerical simulation of stochastic differential equations. SIAM Rev. **43**(3), 525–546 (2001). https://doi.org/10.1137/S0036144500378302
66. World Health Organization, WHO COVID-19 Dashboard, https://data.who.int/dashboards/covid19/cases?m49=356, Accessed: 2024-05-17
67. World Health Organization, WHO Population Data, https://data.who.int/countries/356, Accessed: 2024-05-17
68. Contractor, A., Shivaprakash, S., Tiwari, A., Setia, M.S., Gianchandani, T.: Effectiveness of Covid-19 vaccines (CovishieldTM and Covaxin®) in healthcare workers in Mumbai, India: A retrospective cohort analysis. PLoS ONE **17**(10), e0276759 (2022). https://doi.org/10.1371/journal.pone.0276759
69. Marino, S., Hogue, I.B., Ray, C.J., Kirschner, D.E.: A methodology for performing global uncertainty and sensitivity analysis in systems biology. J. Theor. Biol. **254**(1), 178–196 (2008). https://doi.org/10.1016/j.jtbi.2008.04.011